Deepening and narrowing impacts on circulation, stratification, and sediment transport in the Changjiang Estuary

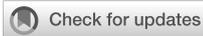Lin, Jianliang; van Prooijen, Bram C.; Zhu, Chunyan; Guo, Leicheng; He, Qing; Wang, Zheng Bing; Yang, Qingshu

Important note
To cite this publication, please use the final published version (if applicable).
Please check the document version above.

Deepening and narrowing impacts on circulation, stratification, and sediment transport in the Changjiang Estuary

Jianliang Lin[1], Bram C. van Prooijen[2], Chunyan Zhu[3], Leicheng Guo[3], Qing He[3]*, Zheng Bing Wang[2,3,4] and Qingshu Yang[1]

[1]Institute of Estuarine and Coastal Research/State and Local Joint Engineering Laboratory of Estuarine Hydraulic Technology, School of Marine Engineering and Technology, Sun Yat-Sen University, Zhuhai, China, [2]Faculty of Civil Engineering and Geosciences, Delft University of Technology, Delft, Netherlands, [3]State Key Laboratory of Estuarine and Coastal Research, East China Normal University, Shanghai, China, [4]Deltares, Delft, Netherlands

Channel deepening and narrowing are common anthropogenic modifications in estuaries, but their combined effects on estuarine circulation, stratification, and sediment transport remain insufficiently understood. This study investigates these combined impacts in the North Passage of the Changjiang Estuary, where large-scale deepening and narrowing have significantly altered hydrodynamic and sediment processes. Our analysis demonstrates that channel deepening intensifies estuarine circulation by strengthening the landward near-bed flow, thereby enhancing sediment import. Contrary to initial expectations that narrowing would promote sediment flushing, our results indicate that narrowing increases stratification, steepens along-estuary salinity gradients, and suppresses vertical mixing. Intensified stratification further reinforces estuarine circulation, promoting sediment trapping at the saltwater intrusion limit. Additionally, enhanced tidal pumping driven by increased velocity and suspended sediment concentration gradients extends the estuarine turbidity maximum both upstream and downstream, a process often overlooked in engineered estuaries. These findings challenge conventional assumptions regarding the sedimentary impacts of narrowing, emphasizing instead its critical role in amplifying estuarine circulation and sediment trapping. Our results provide new insights into sediment dynamics in river-dominated estuaries, with significant implications for estuarine management, dredging operations, water quality control, and long-term morphological stability.

KEYWORDS

estuarine circulation, tidal pumping, density stratification, estuarine turbidity maximum, Changjiang Estuary

1 Introduction

Estuaries, critical transition zones between rivers and oceans, face unprecedented pressures due to human activities aimed at enhancing navigation, flood protection, and land reclamation. Over the past century, large-scale engineering interventions (e.g., channel deepening, narrowing, and diking) have profoundly reshaped estuarine hydrodynamics, sediment transport, and ecological functions (Winterwerp et al., 2013; Talke and Jay, 2020; Guo et al., 2021a; Zhang et al., 2022b, 2023). These modifications often trigger unintended consequences, such as tidal amplification, enhanced stratification, and increased sediment trapping, leading to regime shifts to hyper-turbidity and hypoxia, and thereby degrading water quality and habitat integrity (Talke et al., 2009; Winterwerp and Wang, 2013; Wang et al., 2014; Grasso and Le Hir, 2019; Schmidt et al., 2019; Dijkstra and de Goede, 2024).

Geomorphological evolution plays a critical role in estuarine hydrodynamics and sediment dynamics. Previous studies have shown that morphological changes, including channel migration, delta erosion, and sedimentation, significantly affect estuarine circulation patterns, sediment transport mechanisms, and ecosystem stability. For example, in the Changjiang Estuary, dam-induced reductions in sediment supply have led to delta erosion and significant geomorphic adjustments, altering tidal currents, estuarine circulation, and sediment transport pathways (Yang et al., 2011; Dai et al., 2014; Luan et al., 2016, 2021; Guo et al., 2021a). Similar phenomena have been observed in global estuaries such as the Mississippi Delta, where human interventions and sediment supply reductions substantially influenced hydrodynamic conditions and sedimentary dynamics (Blum and Roberts, 2009; Day et al., 2019; Zhang et al., 2022b). Understanding these geomorphological impacts is essential for accurately predicting estuarine responses to anthropogenic changes and developing sustainable management strategies.

Extensive research has explored the impacts of channel deepening in tide-dominated estuaries, such as the Ems, Seine, and Loire, revealing significant feedback loops between tidal amplification, sediment import via tidal pumping, and sediment-induced drag reduction (Winterwerp et al., 2013; de Jonge et al., 2014; van Maren et al., 2015a, b; Dijkstra et al., 2019b; Grasso and Caillaud, 2023; Dijkstra and de Goede, 2024). However, river-dominated estuaries, where freshwater discharge exerts primary hydrodynamic control, remain poorly understood despite their ecological and economic significance. This knowledge gap hinders predictive modeling and effective adaptive management, particularly in Asia mega-deltas experiencing rapid economic growth and intensified estuarine interventions (Guo et al., 2021a; Chu et al., 2022; van Maren et al., 2023).

In tide-dominated estuaries, channel deepening often triggers regime shifts to hyper-turbid conditions due to tidal pumping-driven sediment import. For instance, the Ems Estuary experienced a 10-fold increase in suspended sediment concentration (SSC) following dredging, driven by a positive feedback loop between tidal asymmetry, sediment import, and sediment-induced drag reduction (Winterwerp and Wang, 2013; van Maren et al., 2015a,

b, Dijkstra et al., 2019a, b). However, such mechanisms may differ significantly in river-dominated estuaries like the Changjiang (Yangtze) Estuary, where river discharge (~28,500 m³/s) overwhelms tidal forcing, with a Canter-Cremers number $N = QT/P \approx 0.5$, where Q is river discharge, T is tidal period, and P is tidal prism (Zhang et al., 2016). Here, estuarine circulation (i.e., the gravitational exchange between seaward freshwater flow and landward saline flow) is typically the main sediment transport driver (Shi, 2004; Liu et al., 2011b; Jiang et al., 2013a; Li et al., 2016). The Deep Waterway Project (DWP) in the Changjiang Estuary, initiated in 1998 to deepen and narrow the North Passage, provides a unique opportunity to study the impact of anthropogenic modifications on stratification and sediment dynamics in such river-dominated systems.

Post-DWP, the North Passage experienced a regime shift from low-turbid to hyper-turbid conditions, with near-bed SSC increasing to 80 kg/m³, approximately twenty times pre-DWP levels, despite a 70% decline in fluvial sediment supply due to upstream dam construction (Wan and Zhao, 2017; Ge et al., 2018; Guo et al., 2019; Lin et al., 2021). However, the evolution of estuarine turbidity maximum (ETM) remains debated. Model results from Song and Wang (2013) indicate a seaward ETM shift due to increased flows, whereas observations by Jiang et al. (2013b) suggest a landward shift and along-estuary extension of ETM post-DWP. Conventional tidal pumping-driven sediment trapping models cannot fully explain this anomaly. Recent evidence points to enhanced estuarine circulation and stratification driven by channel narrowing and deepening as potentially significant drivers of sediment import, independent of tidal mechanisms. After the DWP, intensified estuarine circulation and siltation near the saltwater intrusion limit were observed (Wang et al., 2010; Liu et al., 2011a, 2011b, 2019; Song and Wang, 2013; Li et al., 2016; Wan and Zhao, 2017). Yet, the exact roles of estuarine circulation, tidal pumping, and sediment-induced stratification remain unclear.

Furthermore, recent studies highlight the role of concentrated benthic suspensions in enhancing stratification (Ge et al., 2018; Li et al., 2018; Lin et al., 2021), but the interplay between channel geometry (e.g., depth, width) and these processes needs further investigation. Previous research identified a mud bank in the delta front as a sediment source potentially supporting elevated SSC in the North Passage (Liu et al., 2011b; Li et al., 2016; Zhang et al., 2022a; Zhu et al., 2025). However, the mechanism underlying the sediment import remains uncertain.

This study addresses these gaps by analyzing field measurements collected before and after the DWP in the Changjiang Estuary. We aim to quantify how deepening and narrowing alter estuarine circulation and stratification, identify the dominant sediment import mechanism (estuarine circulation vs. tidal pumping), and characterize the feedback between sediment-induced stratification and turbulence damping. Three specific hypotheses guide our analysis: (1) Channel narrowing enhances estuarine circulation by increasing along-channel salinity gradients and reducing eddy viscosity, contrary to conventional steady-state predictions; (2) Sediment-induced stratification dominates post-DWP conditions, creating a positive feedback loop that suppresses turbulence and promotes near-bed

sediment trapping; (3) Tidal pumping redistributes sediment but does not drive net import in this river-dominated system, distinguishing it from tide-dominated estuaries.

Our findings reveal that the DWP triggered a regime shift toward hyper-turbid conditions, with stratification and sediment import mechanisms distinctively different from those in tide-dominated estuaries. These results challenge the prevailing assumption that narrowing estuaries universally enhances sediment export, offering critical insights into managing sedimentation, hypoxia, and navigation in river-dominated estuaries worldwide. By integrating hydrodynamic theory and observations, this study advances predictive models of estuarine response to human interventions, emphasizing the importance of geometry-specific management strategies.

Following this introduction, Section 2 describes the study area and DWP interventions. Section 3 outlines field measurements, sediment flux decomposition methods, and stratification analysis techniques. Section 4 presents empirical results, including changes in estuarine topography, circulation, and sediment transport. Section 5 discusses mechanistic insights, compares findings with tide-dominated estuaries, and explores implications for estuarine management. Finally, section 6 summarizes key findings and provides policy recommendations for estuary management under intensive engineering interventions.

2 The Changjiang Estuary and Deep Waterway Project

The Changjiang (Yangtze) River, Asia's largest river by discharge, delivers approximately 9×10^3 km³ of freshwater annually to the East China Sea, alongside historically significant sediment loads (Ministry of Water Resources the People's Republic of China, 2024). However, basin-scale anthropogenic interventions, including dam constructions (e.g., the Three Gorges Dam) and soil conservation measures, have reduced riverine sediment supply by 70% since the 1980s, from 470 Mt/yr (1953~1985) to 132 Mt/yr (2003~2015) (Guo et al., 2019; Peng et al., 2020; Wu et al., 2020). The Changjiang Estuary, characterized by a multi-channel system with four outlets (i.e., North Branch, North Channel, North Passage, and South Passage; Figure 1), has evolved under complex interactions between river discharge, tidal forcing, and human interventions. The estuary is within the meso-tidal regime, with a mean tidal range of 2.7 m and a maximum of 5.0 m at Niupijiao (Guo et al., 2015). This dynamic environment supports one of the world's most pronounced ETMs, where SSC exceeds 60 kg/m³ (Wan and Zhao, 2017; Lin et al., 2021).

To accommodate growing maritime trade, the DWP was initiated in 1998 to transform the North Passage into a 12.5-m-deep navigational channel. Executed in three phases (8.5 m by 2002, 10.0 m by 2005, and 12.5 m by 2010), the DWP involved constructing two 50-km training dikes, 19 transverse groins, and continuous maintenance dredging. These interventions enhanced saltwater intrusion and stratification, leading to ETM evolution (Wang et al., 2010; Jiang et al., 2013b; Song and Wang, 2013; Zhu et al., 2018a, 2021b; Chen et al., 2020). Near-bed SSC in the ETM surged to 80 kg/m³, despite declining riverine sediment supply (Wan and Zhao, 2017; Ge et al., 2018; Guo et al., 2019; Lin et al.,

2021). Surface SSCs, however, decreased significantly (Lin et al., 2021; Luo et al., 2022). Consequently, sediment-induced density gradients (i.e., stratification) were notably enhanced (Li et al., 2018), which may overwhelm salinity-driven density stratification.

3 Materials and methods

3.1 Datasets

To assess the impact of the DWP on estuarine stratification and sediment transport, we analyzed field measurements collected from the North Passage of the Changjiang Estuary before (June 1999) and after (August 2012) the project. These measurements, conducted during spring tides, were obtained from campaigns conducted by the Changjiang Estuary Waterway Administration Bureau. The pre-DWP dataset (1999) includes data from four monitoring stations, whereas the post-DWP dataset (2012) comprises an expanded network of nine stations (Figure 1; Table 1).

Hydrological conditions during the two surveys were comparable, facilitating a meaningful analysis of DWP impacts. During the observations, the mean river discharge at the Datong hydrological station was 54,300 m³/s in 1999 and 52,500 m³/s in 2012, differing by less than 3%. Similarly, tidal ranges were closely matched, with observed ranges of approximately 3.3 m in 1999 and 3.7 m in 2012. Despite this consistency in hydrological and tidal conditions, the fluvial sediment load declined significantly between these two periods, from approximately 340 Mt/yr in 1999 to 132 Mt/yr in 2012, as a direct consequence of extensive sediment retention in upstream reservoirs and improved soil conservation practices in the watershed (Guo et al., 2018, 2019; Zhu et al., 2019).

At each monitoring station, hydrodynamic and sedimentary parameters were measured at six relative-depth layers, specifically at normalized depths (z/H) of 0.05 (near-bed), 0.2, 0.4, 0.6, 0.8, and 0.95 (near-surface), where H represents the total water depth and z is the vertical distance above the seabed. Flow velocities and directions were measured every 30 minutes using rotor current meters, with accuracies of ±0.01 m/s for velocity and ±1° for direction. Water samples were collected every 30 minutes at each depth layer to determine salinity and SSC. Salinity was measured using a calibrated salimeter with a precision of ±0.01 PSU. SSC was determined by filtering water samples through pre-weighed membrane filters, followed by drying at 60°C for eight hours and weighing to quantify the sediment mass. These measurements were tidally averaged directly from the observed data for subsequent analyses, without applying harmonic analysis or additional preprocessing.

3.2 Sediment flux decomposition

In this study, we applied a sediment flux decomposition approach to understand changes in sediment transport mechanisms induced by the DWP. The instantaneous along-estuary velocity (u) and SSC (c) at any depth can be divided into tide-averaged and oscillatory components, and the tide-averaged
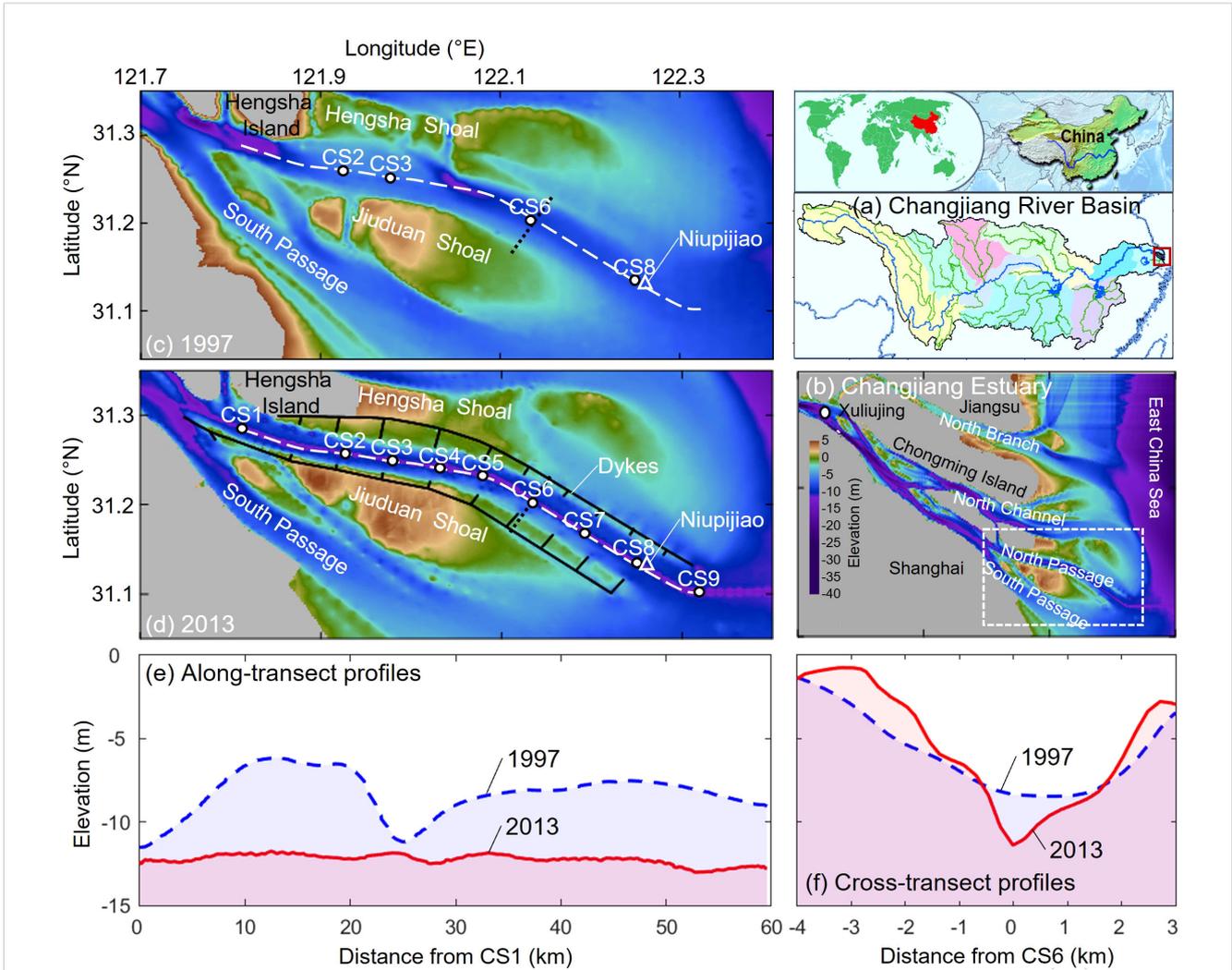
FIGURE 1
The Changjiang Estuary and its bathymetry changes between 1997 (pre-DWP) and 2013 (post-DWP). DWP: Deep Waterway Project. **(a)** The location of the Changjiang Estuary in the Changjiang River Basin, China. **(b)** Map of the Changjiang Estuary. The bathymetry of the North Passage in 1997 **(c)** and 2013 **(d)**. Elevation is referenced to the Theoretical Depth Datum. The black lines indicate the Deepwater Navigational Channel, while white dots represent observation stations. The triangle marks the tide gauging station at Niupijiao. Along-estuary transects (white dashed lines) and cross-estuary transects (black dotted lines) are illustrated in panels **(e, f)**, respectively. Positive x is oriented seaward along the channel, and positive y extends across the channel to the northeast.

term can be further decomposed into a depth-averaged component and its deviation (Dyer, 1974; Su and Wang, 1986; Zhu et al., 2022), as Equations 1 and 2:

$$u = \overline{u_0} + u_0' + u_t \qquad (1)$$

$$c = \overline{c_0} + c_0' + c_t \qquad (2)$$

where $\overline{u_0}$ and $\overline{c_0}$ Represent tidally depth-averaged values, u_0' and c_0' denote vertical deviations from tidally averaged values, and u_t and c_t denote tidal oscillation. The residual (net) sediment flux is obtained as Equation 3:

$$\langle uc \rangle = \underbrace{\langle \overline{u_0}\,\overline{c_0} \rangle}_{1} + \underbrace{\langle u_0' c_0' \rangle}_{2} + \underbrace{\langle u_t c_t \rangle}_{3} + \underbrace{\langle \overline{u_0}\, c_0' \rangle}_{4} + \underbrace{\langle u_0'\, \overline{c_0} \rangle}_{5} \qquad (3)$$

where the brackets represent tidal averaging, the first term denotes advection by mean flow (i.e., barotropic component or non-tidal drift), the second term accounts for transport driven by estuarine circulation, and the third term represents tidal pumping. These components were analyzed to assess the relative contributions of different sediment transport mechanisms before and after the DWP. The last two terms produce no residual sediment fluxes, as their integrals over the water column equal zero.

3.3 Stratification and potential energy anomaly

The influence of the DWP on vertical density stratification was evaluated using the potential energy anomaly (φ), a metric

Observation period	Stations	Tidal range* (m)	Discharge** (m^3/s)
18:00, 29 June, 1999 -10:00, 30 June, 1999	CS2, CS3, CS6, CS8	3.3	54,300
05:00, 17 August, 2012 - 19:00, 17 August, 2012	CS1-CS9, CS6s, CS6n	3.7	52,500

* Tidal range measured at the mouth of the estuary (Niupijiao Tide Gauging Station);
** Monthly mean river discharge at the tidal limit (Datong Hydrological Gauging Station).

representing the energy required to mix the water column into a uniform density profile (Simpson et al., 1990). The potential energy anomaly is defined as Equation 4:

$$\varphi = \frac{1}{H} \int_0^H (\bar{\rho} - \rho)gzdz \qquad (4)$$

where ρ is the water density, $\bar{\rho}$ is the depth-averaged density, g is gravitational acceleration, H is water depth, and z is the vertical coordinate.

Water density was determined from salinity, temperature, and SSC using Equation 5:

$$\rho = \rho_w(T, \ S) + \left(1 - \frac{\rho_w}{\rho_s}\right)C \qquad (5)$$

where $\rho_w(T, \ S)$ is the density of freshwater, ρ_s is the density of suspended sediments (estimated as 2,570 kg/m^3 for the Changjiang Estuary; Guo et al., 2017), and C is SSC. Since temperature variations were minimal (<1°C) during observations, temperature effects were neglected.

To examine the temporal evolution of stratification, we evaluated the rate of change of φ (Simpson et al., 1990), using Equation 6:

$$\frac{\partial \varphi}{\partial t} = \frac{g}{H} \int_0^H \frac{\partial (\bar{\rho} - \rho)}{\partial t} zdz \qquad (6)$$

where t denotes time. Accounting for only the along-estuary direction (x), Simpson et al. (1990) proposed the classical tidal straining, as Equation 7:

$$\frac{\partial \varphi}{\partial t} = \frac{g}{H} \frac{\partial \bar{\rho}}{\partial x} \int_0^H (u - \bar{u})zdz \qquad (7)$$

where u is along-estuary velocity, and $\bar{u}$ is its vertically averaged value.

This formulation can be extended to three dimensions (Burchard and Hofmeister, 2008; de Boer et al., 2008), as Equation 8:

$$\frac{\partial \varphi}{\partial t} = \frac{g}{H} \int_0^H (\underbrace{\bar{u}\frac{\partial \tilde{\rho}}{\partial x}}_{A_x} + \underbrace{v\frac{\partial \tilde{\rho}}{\partial y}}_{A_y} + \underbrace{\tilde{u}\frac{\partial \bar{\rho}}{\partial x}}_{S_x} + \underbrace{\tilde{v}\frac{\partial \bar{\rho}}{\partial y}}_{S_y} + R)zdz \qquad (8)$$

where x, y, and z represent along-estuary, cross-estuary, and vertical directions, respectively. The above horizontal and wavy lines denote depth-averaged value and deviation, respectively. This formulation allows for the identification of processes such as advection (A_x and A_y), straining (S_x and S_y), which are essential for understanding estuarine circulation and sediment transport dynamics. Since advection and straining are primary contributors to water stratification, and the remaining (R) contribution is negligible (de Boer et al., 2008), we focus on advection and straining processes in this work.

3.4 Eddy viscosity and mixing

Vertical mixing was assessed using eddy diffusivity (k_t), linked to eddy viscosity (v_t) with the turbulent Prandtl-Schmidt number. Eddy viscosity quantifies momentum transfer due to turbulent eddies. Following Munk and Anderson (1948), v_t was estimated as Equation 9:

$$v_t = \kappa u_\star z \left(1 - \frac{z}{H}\right)(1 + 10Ri)^{-\frac{1}{2}} \qquad (9)$$

where κ is von Kármán's constant (0.41), and $u_\star$ is the friction velocity, estimated by the regression of von Kármán-Prandtl velocity profile, as Equation 10:

$$u = \frac{u_\star}{\kappa} \ln\left(\frac{z}{z_0}\right) \qquad (10)$$

where z_0 is hydraulic roughness. Both $u_\star$ and z_0 were estimated with a regression coefficient $R^2 > 0.80$. The gradient Richardson number (Ri) is defined as Equation 11:

$$Ri = -\frac{g}{\rho}\frac{\partial \rho}{\partial z} / \left[\left(\frac{\partial u}{\partial z}\right)^2 + \left(\frac{\partial v}{\partial z}\right)^2\right] \qquad (11)$$

Eddy viscosity was vertically and tidally averaged to assess its role in estuarine circulation following Hansen and Rattray (1965) and MacCready and Geyer (2010). The relationship between stratification and estuarine circulation intensity (U_e) was evaluated using Equation 12:

$$U_e = \frac{1}{48}\frac{\beta_s gH^3}{K_M}\frac{\partial S}{\partial x} \qquad (12)$$

where β_s is the saline contraction coefficient, H is water depth, K_M is vertically averaged eddy viscosity, and $\frac{\partial S}{\partial x}$ is the along-channel salinity gradient. By applying these calculations to pre- and post-DWP datasets, we assessed the influence of deepening and narrowing on estuarine circulation.

4 Results

4.1 Topographic changes

Due to the DWP, the North Passage underwent significant morphological alterations, including channel deepening and narrowing. To evaluate these changes, we compared the estuarine topography before (1997) and after (2013) the completion of the DWP (Figure 2). The modifications primarily affected channel depth, estuary width, and cross-sectional area along the North Passage.

Bathymetric surveys indicate that the navigation channel deepened substantially throughout the estuary, with the most pronounced changes occurring in the upper reaches (between CS2 and CS3), where the thalweg depth increased by over 70% (Figure 2c). Further downstream, between CS6 and CS9, depth increases ranged from 40% to 60%. Correspondingly, the mean depth of cross-sections doubled at CS2 and increased by 10%~60% at other locations (Figure 2b). These changes reflect natural sediment redistribution and anthropogenic dredging efforts to maintain navigability.

Despite the increased depth, the total cross-sectional area of the North Passage decreased due to channel narrowing. The width of the estuary contracted by 10%~70% along different segments, with the most significant reductions observed in the downstream sections (Figure 2d). As a result, cross-sectional areas decreased

progressively seaward, with reductions ranging from approximately 10% at CS1 to nearly 50% at CS8 (Figure 2a).

Overall, the DWP led to a deeper and narrower estuarine channel, fundamentally altering the hydrodynamic conditions. These topographic changes have implications for estuarine circulation, salinity stratification, and sediment transport, which are analyzed in subsequent sections.

4.2 Velocity, salinity, and SSC changes

The hydrodynamic conditions in the North Passage changed notably after the DWP, primarily due to channel deepening and narrowing. These modifications influenced flow velocity, salinity intrusion, and SSC, altering the estuarine circulation and stratification.

4.2.1 Velocity changes

As a consequence of channel narrowing, flow velocities increased significantly throughout the North Passage. The maximum recorded velocity rose from 2.8 m/s before the DWP to 3.2 m/s after the DWP. The most pronounced acceleration occurred in the upper reaches of the estuary and near the surface. At CS3, for example, the peak depth-averaged ebbing velocity increased from 1.8 m/s pre-DWP to 2.8 m/s post-DWP, whereas flood velocities remained relatively stable around 0.9 m/s.
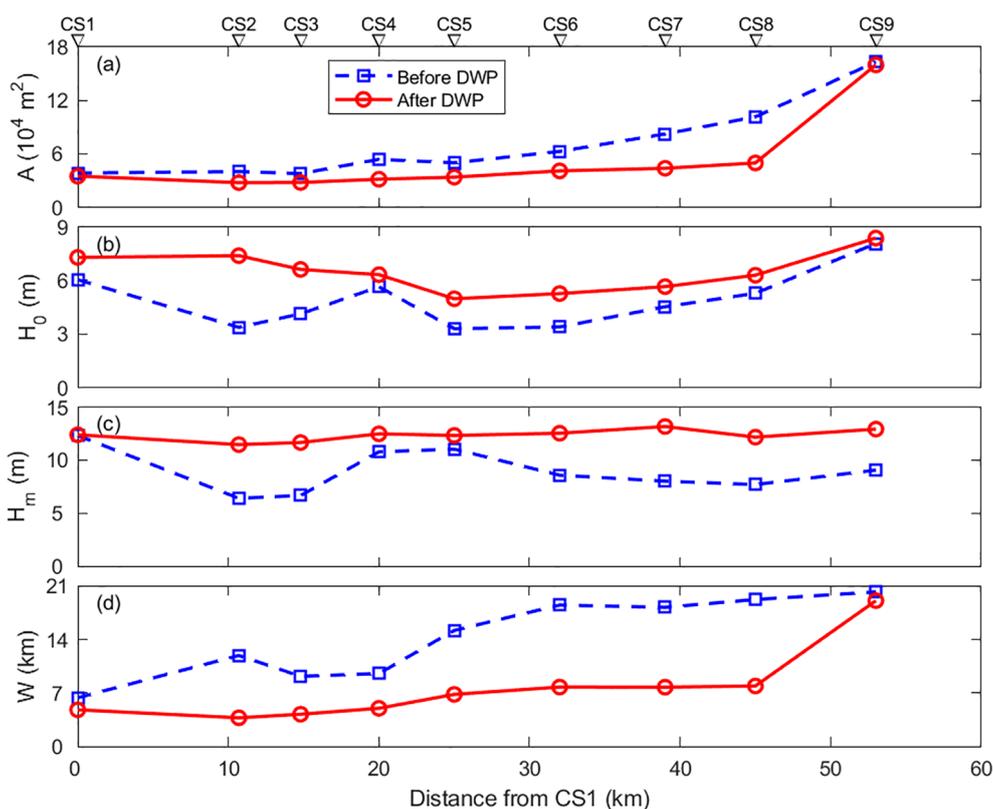

FIGURE 2
Topographic changes along the North Passage. **(a)** Cross-sectional area as a function of distance from CS1 before (1997) and after (2013) the Deep Waterway Project (DWP). **(b)** Mean depth of each cross-section. **(c)** Thalweg depth. **(d)** Channel width of the North Passage.

Concurrently, the duration of ebb tides lengthened slightly, from 7.8 hours to 8.1 hours, while flood tide duration reduced from 4.7 hours to 4.4 hours. These changes indicate an enhanced ebb-dominant flow regime (Figure 3), significantly affecting sediment transport and stratification dynamics.

Notably, channel narrowing intensified tidal asymmetry, characterized by a stronger and slightly longer ebb tide relative to the flood tide. Enhanced ebb dominance implies increased seaward sediment transport capacity near the surface layers. However, the intensified vertical velocity shear, resulting from increased ebb velocities near the surface and relatively stable flood velocities near the bed, promotes stratification and enhances turbulence suppression, affecting the vertical distribution of sediment. Thus, the observed tidal asymmetry post-DWP not only intensifies the ebb-dominant sediment transport near the surface but also reinforces near-bed sediment retention through increased stratification and suppressed vertical mixing.

4.2.2 Changes in salinity distribution

The extent of saltwater intrusion remained relatively unchanged after the DWP, with the 5 PSU contour consistently fluctuating between CS6 during low water slack and CS3 at high water slack (Figure 3). However, salinity increased notably near the estuary mouth, particularly near the bottom. For instance, the 20 PSU contour, previously extending only up to CS8, shifted approximately 10 km upstream to CS6 after the DWP. This enhancement in bottom-layer salt intrusion contrasts with reduced surface salinity due to enhanced freshwater outflows. The resulting amplification of vertical salinity gradients increased stratification, as quantified further in Section 4.5.

It should be noted that tidal fluctuations were similar (3.3 m pre-DWP vs. 3.7 m post-DWP), suggesting minimal impact on observed salinity differences. The changes in salinity are thus predominantly due to the alterations in channel geometry rather than differences in tidal conditions. Although detailed wind data were unavailable, seasonal winds typically have minor effects on surface salinity in the Changjiang Estuary. Future studies should explicitly include wind forcing to clarify these interactions better.

4.2.3 Changes in SSC

The ETM expanded significantly following the DWP, with an increase in both its spatial extent and SSC magnitude. The
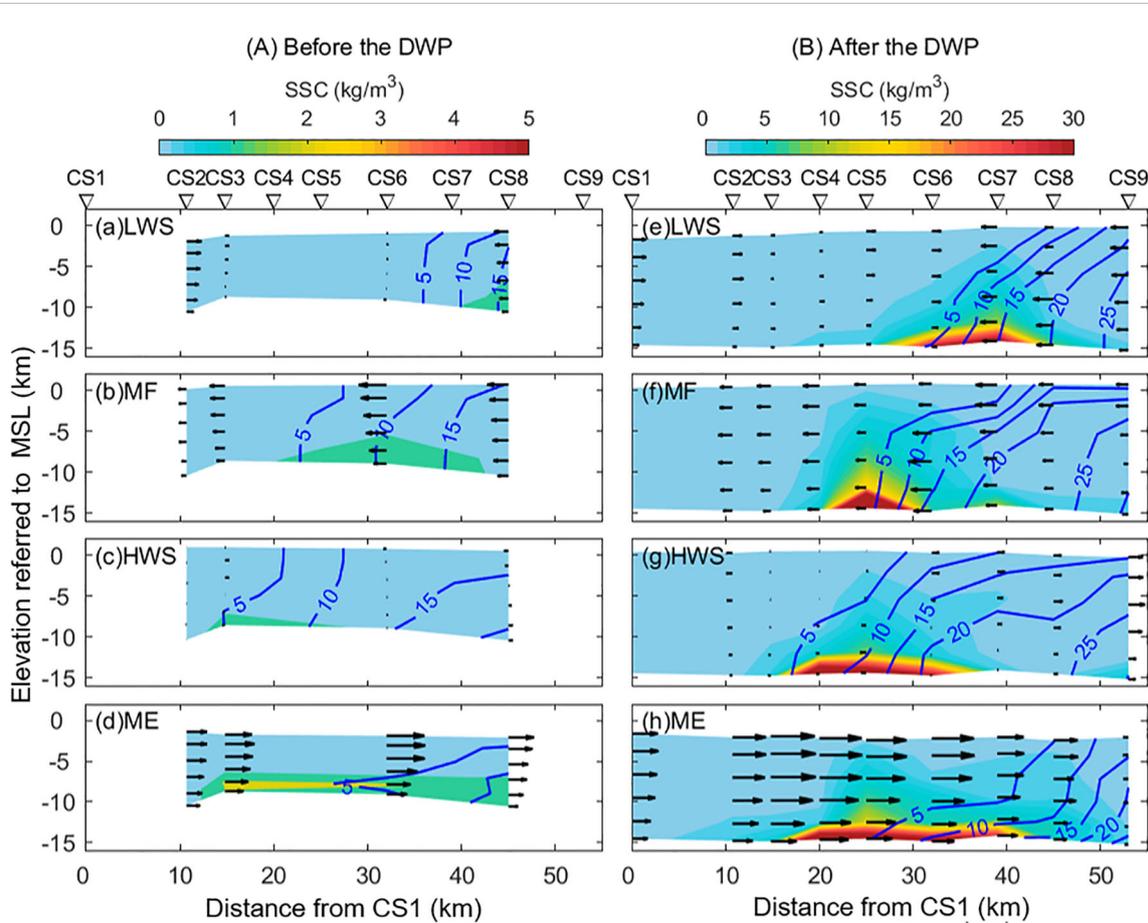
FIGURE 3
Along-estuary distributions of velocity (arrows), salinity (contour lines), and suspended sediment concentration (SSC; filled contours) at different tidal phases: **(a, e)** low-water slack (LWS), **(b, f)** maximum flood (MF), **(c, g)** high-water slack (HWS), and **(d, h)** maximum ebb (ME). Left panels represent conditions before the Deep Waterway Project (DWP), while right panels show conditions after the DWP. Note that different color bars are used for the left and right panels. MSL, mean sea level.

maximum SSC increased from less than 5 kg/m³ before the DWP to 88 kg/m³ afterward, particularly near the bottom (Figure 3). Throughout the tidal cycle, the ETM exhibited a more extensive distribution, increasing in length from approximately 30 km before the DWP to ~45 km after the DWP—an expansion of 50%. Despite this spatial increase, the ETM remained centered near the saltwater intrusion limit, where sediment convergence occurs due to estuarine circulation and tidal pumping processes.

4.3 Residual flows and estuarine circulation

The DWP significantly altered the residual flow patterns in the North Passage, particularly affecting estuarine circulation. A comparison of conditions before and after the DWP reveals notable changes in flow structure, including an increase in residual currents and the development of enhanced two-layer circulation.

4.3.1 Changes in residual flow patterns

Before the DWP, residual flow was predominantly directed seaward throughout most of the North Passage, with velocities decreasing downstream (Figure 4a). Flow magnitude also varied vertically, with stronger seaward residual currents near the surface (0.6 m/s at CS2) and weaker flows near the bottom (0.4 m/s). At downstream locations, such as CS8, the residual flow was nearly uniform throughout the water column, with an average velocity of 0.1 m/s.

After the DWP, residual flows increased significantly across the estuary, especially near the surface (Figure 4g). At CS6, for instance, surface residual flow nearly doubled from 0.6 m/s to 1.2 m/s. Furthermore, a landward-directed residual flow developed at the mouth of the estuary (CS9), indicating the emergence of a residual circulation cell. This suggests that the estuarine flow regime transitioned from a simple seaward-directed pattern to a more complex two-layer exchange system.

4.3.2 Enhanced estuarine circulation

The strength of estuarine circulation, as indicated by exchange flow intensity, increased notably after the DWP (Figure 5a). Estuarine circulation is typically characterized by seaward-directed flow in the surface layers and landward-directed flow near the bottom, driven by density gradients and gravitational forces. Prior to the DWP, exchange flow velocities were generally low, with U_e values below 0.1 m/s. Following the DWP, U_e values increased to approximately 0.3 m/s, particularly in the mid-to-lower reaches of the estuary. The largest increases were observed at CS6 and CS8, where U_e tripled compared to pre-DWP conditions.

These findings suggest that the combination of channel deepening and narrowing intensified estuarine circulation. The mechanisms responsible for this enhancement include increased stratification, changes in salinity gradients, and modifications in vertical mixing patterns. Subsequent sections discuss the implications of these circulation changes for sediment transport and estuarine dynamics.

4.4 Stratification

The DWP significantly altered the stratification dynamics of the North Passage, intensifying vertical density gradients. To quantify these changes, we analyzed the potential energy anomaly (φ), a measure of the energy required to mix the water column thoroughly. The results indicate that both salinity- and sediment-induced stratification increased after the DWP, with profound implications for estuarine circulation and sediment transport.

4.4.1 Changes in salinity-induced stratification

Before the DWP, stratification in the North Passage was relatively weak, with φ values generally below 100 J/m³. Salinity was the dominant contributor to density differences, particularly in the lower estuary, where saltwater intrusion influenced the vertical structure. During flood tides, the water column became progressively more stratified as denser saline water moved landward. However, this stratification was periodically disrupted during ebb tides due to the retreat of the salt wedge, leading to well-mixed conditions (Figure 6a).

Following the DWP, salinity stratification intensified, particularly in the downstream sections of the estuary. The maximum φ values increased to approximately 220 J/m³, nearly doubling compared to pre-DWP conditions (Figure 6b). The development of stronger and more persistent stratification was primarily driven by enhanced saltwater intrusion near the bottom, while freshwater flushing near the surface maintained vertical density gradients. As a result, stratification was sustained for longer periods over the tidal cycle, influencing turbulence and mixing dynamics.

4.4.2 Changes in sediment-induced stratification

In addition to salinity effects, sediment-induced stratification became a key factor in the post-DWP environment. The concentration of suspended sediment near the bed increased substantially, leading to the formation of dense bottom layers with high SSC. In the mid-estuary region (CS4–CS7), sediment-induced stratification became more significant than salinity stratification, with φ values exceeding 700 J/m³ in these areas (Figure 6e).

Unlike salinity-driven stratification, which primarily followed the tidal cycle, sediment-induced stratification exhibited a different temporal pattern. Peak sediment stratification occurred during periods of accelerating or decelerating flow, likely due to the combined effects of sediment resuspension and deposition. The tidally averaged sediment-induced φ after the DWP increased more than 30-fold compared to pre-DWP values, reaching up to 330 J/m³. This substantial increase implies a greater energy requirement for vertical mixing, further dampening turbulence and reinforcing estuarine circulation.

4.4.3 Implications for mixing and circulation

The enhanced stratification observed after the DWP directly influenced vertical mixing processes. The increase in the
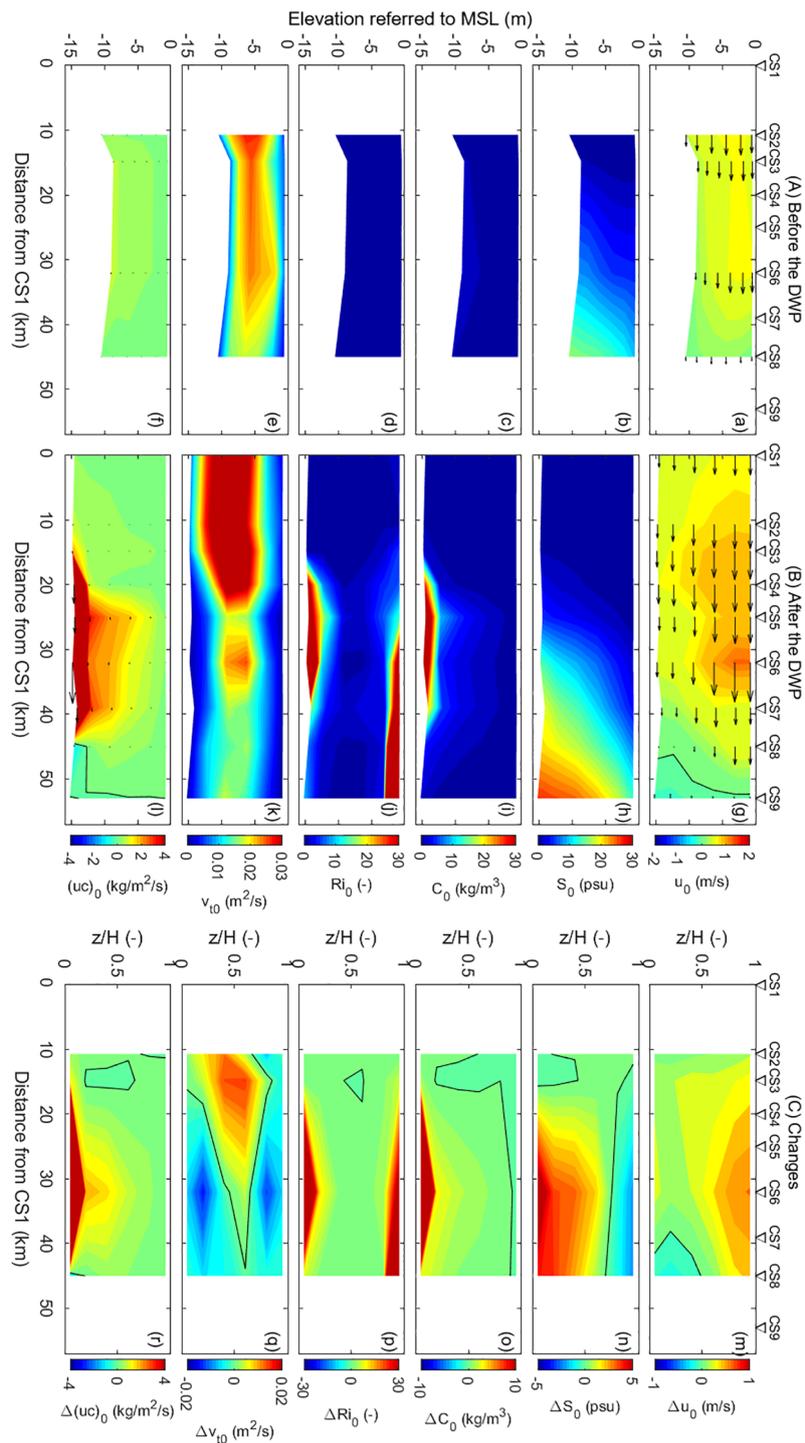
FIGURE 4

-channel distributions of **(a, g)** residual flow, **(b, h)** tidally averaged salinity, **(c, i)** suspended sediment concentration, **(d, j)** Richardson number (Ri), **(e, k)** eddy viscosity, and **(f, l)** residual sediment flux before **(a−f)** and after **(g−l)** the Deep Waterway Project (DWP). Panels **(m−r)** represent the differences between pre- and post-DWP conditions. Positive values for residual flow and sediment flux indicate seaward transport along the channel. Black contour lines denote zero values.

Richardson number (*Ri*) (Figure 4j) indicates stronger suppression of vertical turbulence, particularly in mid-estuarine sections where *Ri* values exceeded 4.0, more than 30 times higher than pre-DWP conditions. Correspondingly, eddy viscosity was reduced by 30%

~40% (Figure 5c), highlighting the damping effect of stratification on turbulent mixing.

A stronger stratification developed during the early flood tide at CS8 (Figures 7, 8). Two processes are responsible for this
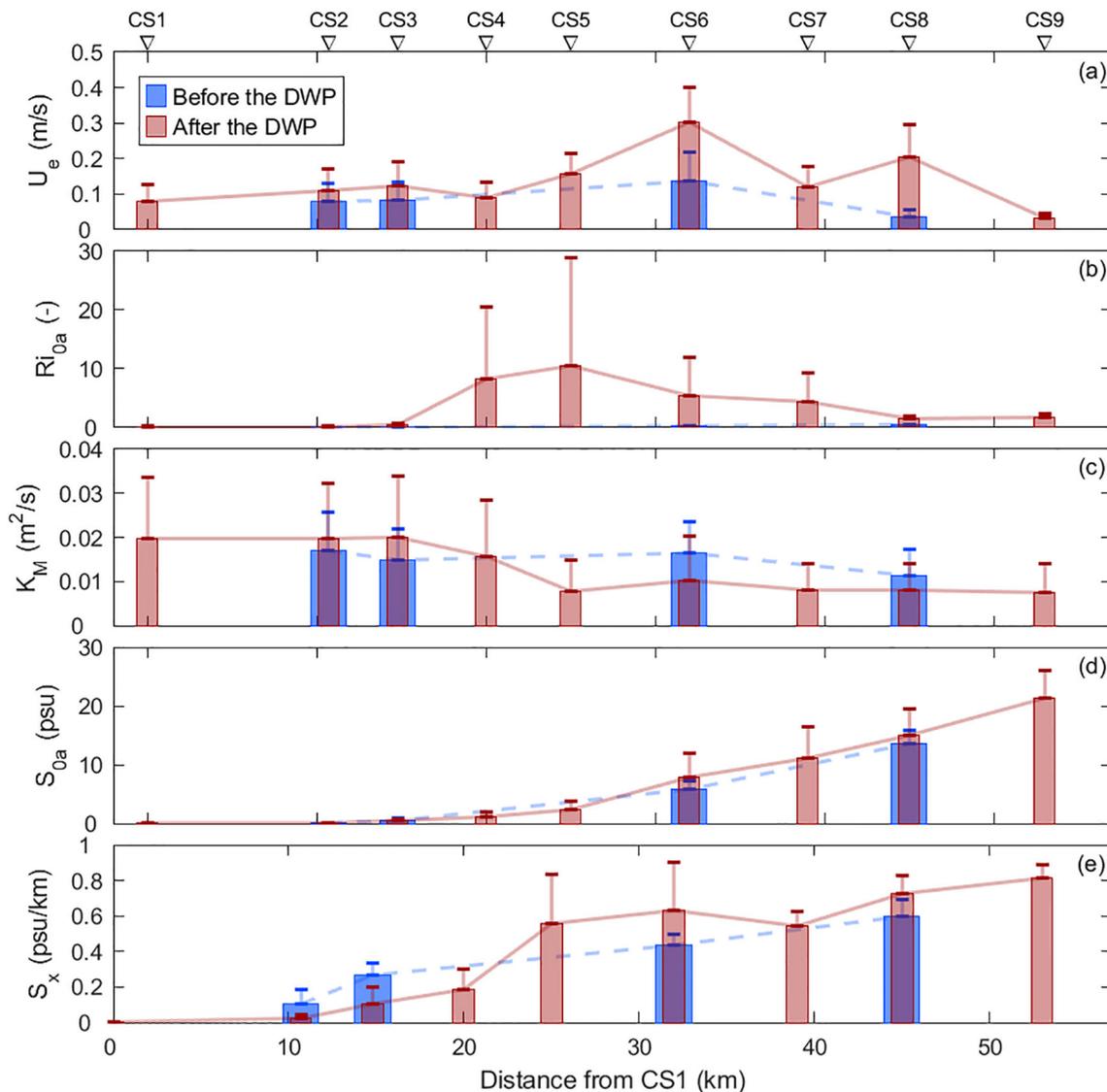
FIGURE 5
Along-channel distributions of vertically and tidally averaged **(a)** exchange flow (U_e), **(b)** Richardson number (Ri_{0a}), **(c)** eddy viscosity (K_M), **(d)** salinity (S_{0a}), and **(e)** along-channel salinity gradient (S_x) before and after the Deep Waterway Project (DWP). Error bars represent standard deviations.

unexpected stratification. First, reversed velocity shears (i.e., straining) moved bottom saltwater landward faster than freshwater near the surface during the early flood tide (Figure 7b). Such stratification development driven by along-channel straining is confirmed by the change rate of salinity-induced potential energy anomaly (Figure 8c). Second, lateral straining and advection also develop stratification during the early flood tide (Figure 8).

Overall, these findings suggest that the combined effects of increased salinity stratification and sediment-induced density gradients played a critical role in modifying estuarine circulation. The suppression of turbulence enhanced the stability of near-bed sediment suspensions, influencing sediment transport pathways and ETM formation, as discussed in subsequent sections.

4.5 Sediment transport

The DWP substantially modified sediment transport dynamics in the North Passage, leading to increased sediment import, intensified ETM formation, and altered transport mechanisms. The primary changes include enhanced residual sediment flux, greater near-bed sediment convergence, and a shift in the relative contributions of different transport processes.

4.5.1 Changes in residual sediment flux

Before the DWP, residual sediment transport was predominantly directed seaward, with a higher SSC near the bottom than at the surface. The maximum residual sediment
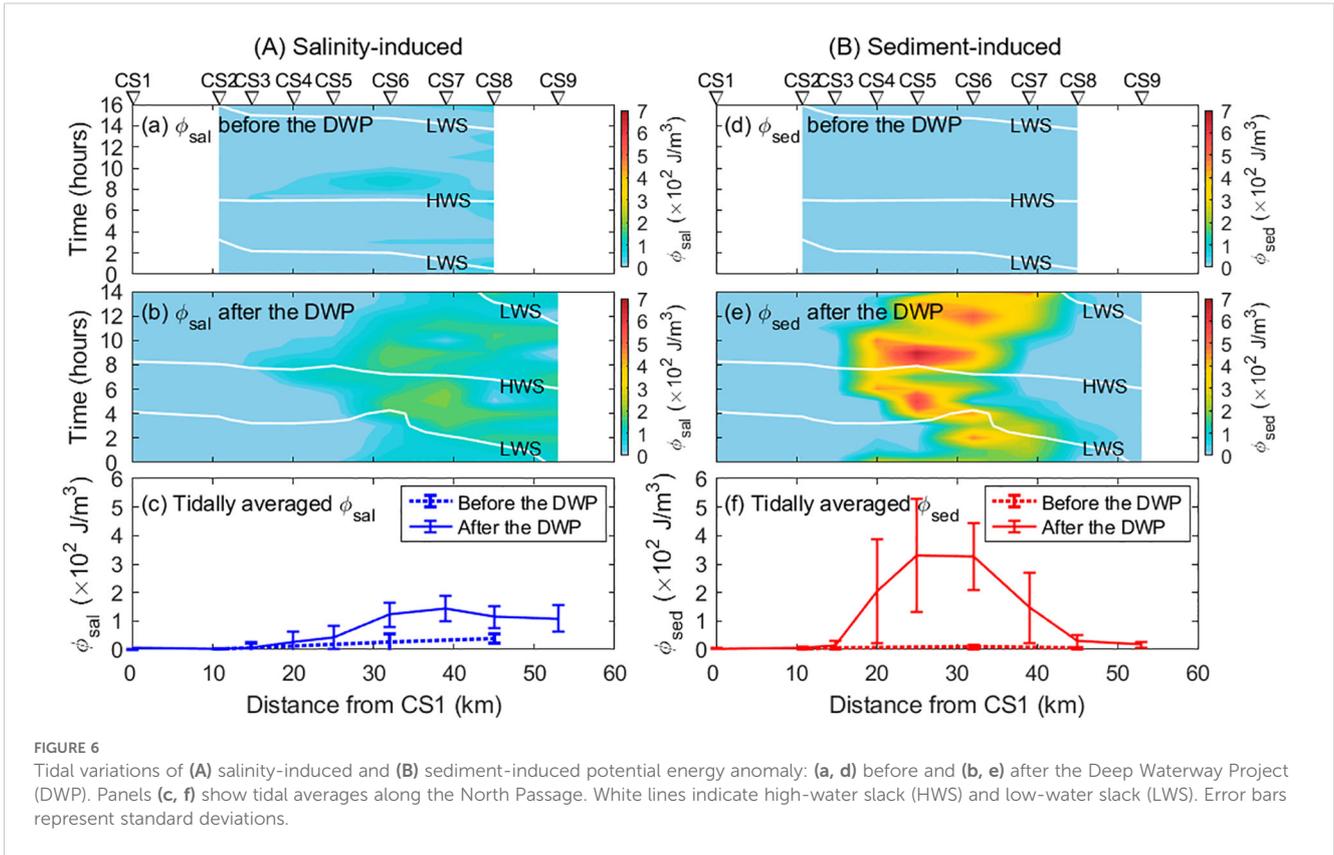
FIGURE 6
Tidal variations of **(A)** salinity-induced and **(B)** sediment-induced potential energy anomaly: **(a, d)** before and **(b, e)** after the Deep Waterway Project (DWP). Panels **(c, f)** show tidal averages along the North Passage. White lines indicate high-water slack (HWS) and low-water slack (LWS). Error bars represent standard deviations.
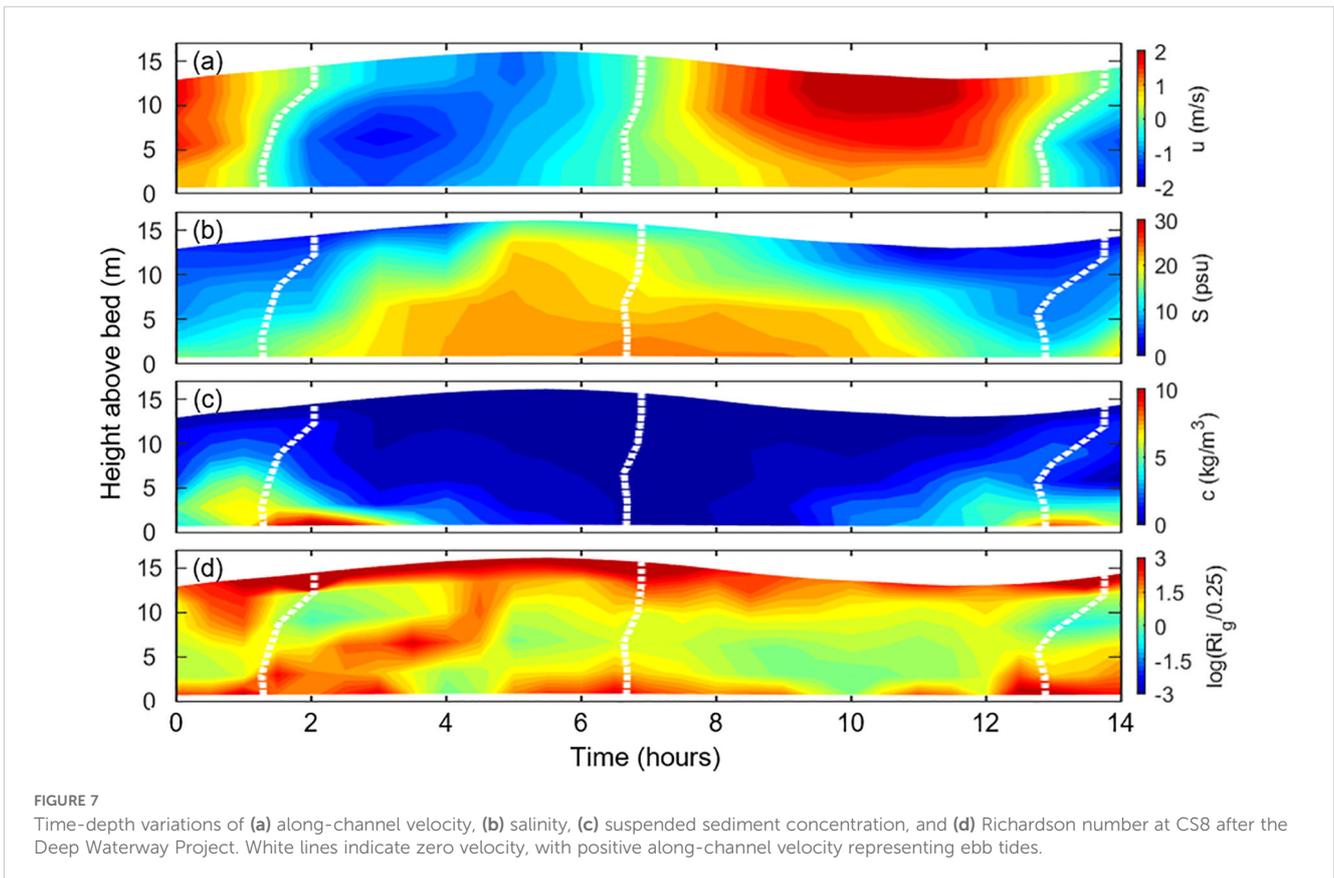

FIGURE 7
Time-depth variations of **(a)** along-channel velocity, **(b)** salinity, **(c)** suspended sediment concentration, and **(d)** Richardson number at CS8 after the Deep Waterway Project. White lines indicate zero velocity, with positive along-channel velocity representing ebb tides.
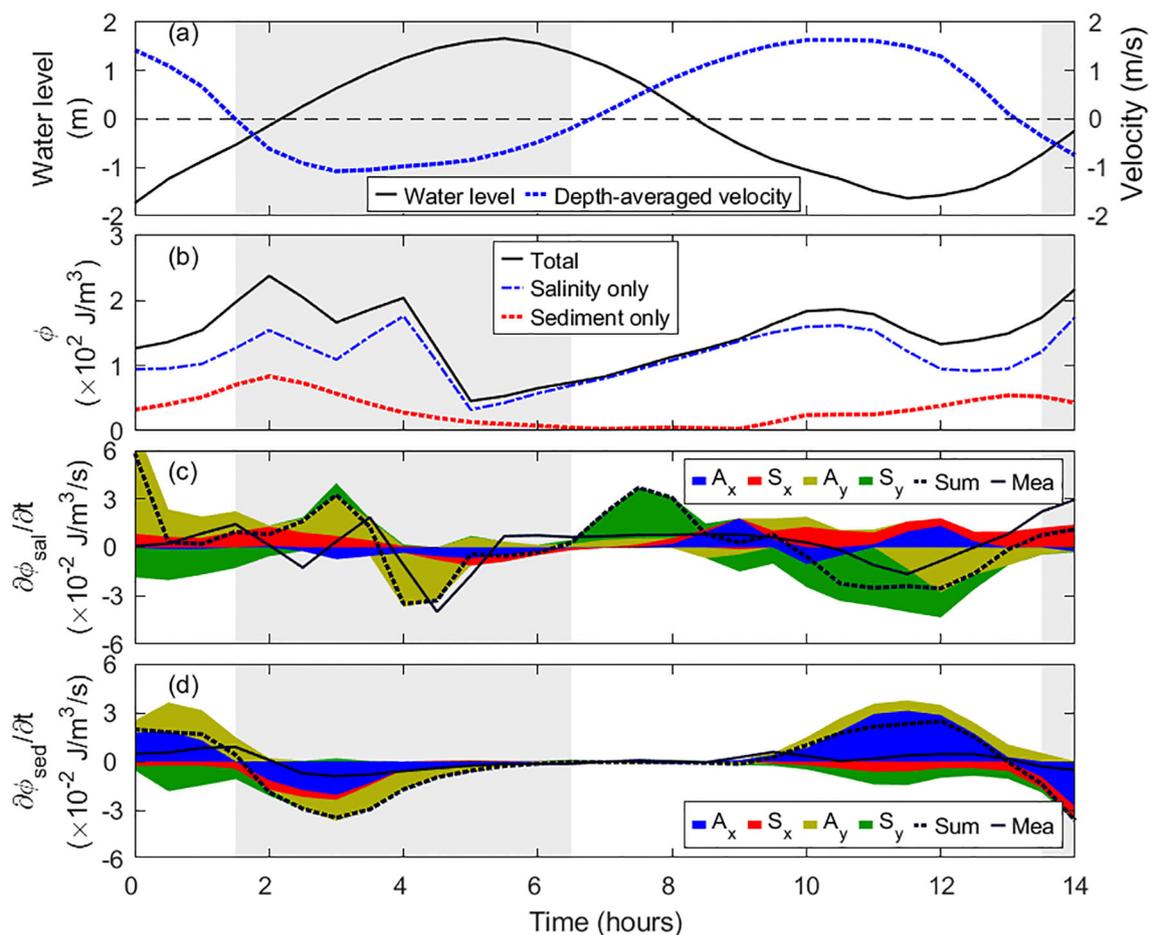
FIGURE 8
Time series of **(a)** water level and depth-averaged velocity, **(b)** potential energy anomaly induced by salinity, sediment, and their combination, and contributions of different terms (i.e., A_x: along-estuary advection, A_y: cross-estuary advection; S_x: along-estuary straining; S_y: cross-estuary straining) to the change rate of **(c)** salinity-induced and **(d)** sediment-induced potential energy anomaly at CS8 after the Deep Waterway Project (DWP). Stacked areas represent the contributions of individual terms, where the sum of positive and negative areas at each time step gives the calculated change rate of potential energy anomaly (dashed lines). Solid lines denote the measured change rate, obtained by computing the time derivative of potential energy anomaly at 30-minute intervals. Gray shading indicates flood tides.

flux prior to the DWP was approximately 0.5 kg/m²/s near the bed, with a decreasing trend from upstream to downstream (Figures 4f, 9a). This pattern suggested a natural trapping mechanism at the saltwater intrusion limit, although the magnitude of sediment retention was relatively low.

Following the DWP, residual sediment transport intensified, particularly near the bottom, where values exceeded 10.0 kg/m²/s in the middle reaches of the estuary (Figures 4l, 9b). This dramatic increase was driven by the formation of high-concentration near-bed suspensions, where SSCs reached up to 80 kg/m³. While residual transport remained seaward at upstream stations (e.g., CS1–CS6), a clear landward transport component emerged near the mouth (CS8), resulting in sediment convergence at the saltwater intrusion limit. This convergence played a crucial role in the expansion of the ETM.

4.5.2 Decomposition of sediment transport mechanisms

To better understand the processes controlling sediment transport, the total sediment flux was decomposed into its primary components: advection (barotropic and estuarine circulation-driven transport) and tidal pumping.

Before the DWP, advection was the dominant transport mechanism, controlled mainly by river discharge. Barotropic transport accounted for most sediment flux, while estuarine circulation and tidal pumping contributions were relatively minor (Figures 9a, 10a).

After the DWP, estuarine circulation and tidal pumping became more influential (Figures 9b, 10b). Near the bottom, estuarine circulation facilitated significant landward sediment transport, with fluxes reaching 15 kg/m²/s. Meanwhile, tidal pumping,
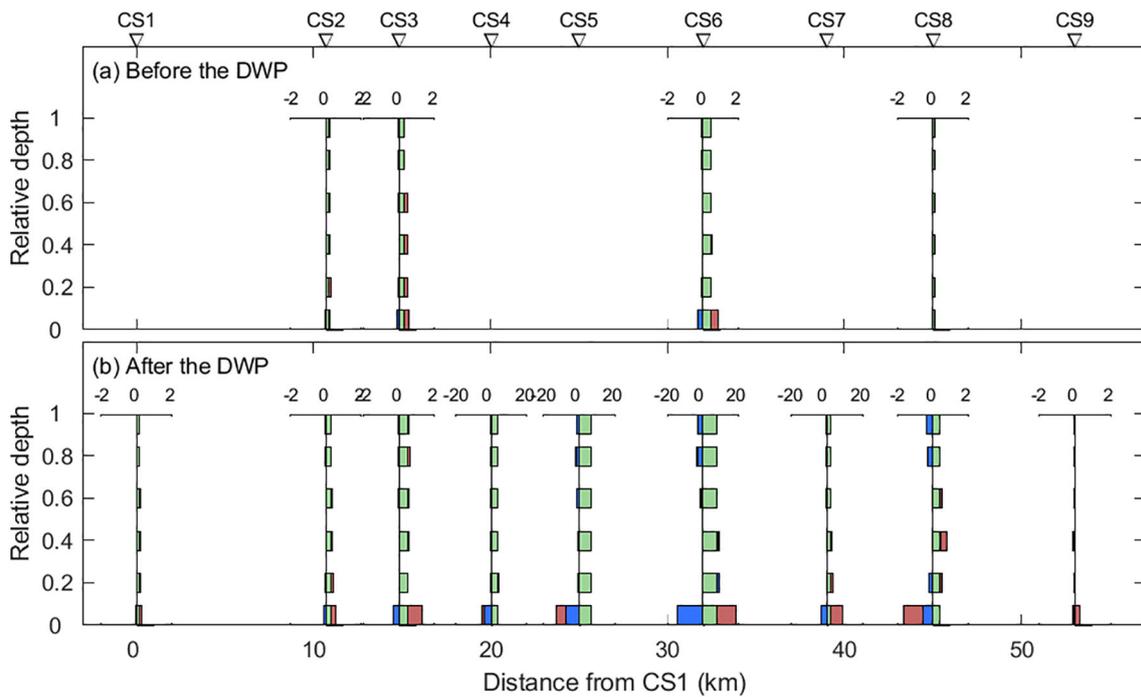
FIGURE 9
Along-channel sediment fluxes driven by barotropic (green), estuarine circulation (blue), and tidal pumping (brown) components **(a)** before and **(b)** after the Deep Waterway Project (DWP). Positive values indicate seaward transport, while negative values represent landward transport. Note the different scales in the lower panel for CS4, CS5, CS6, and CS7.

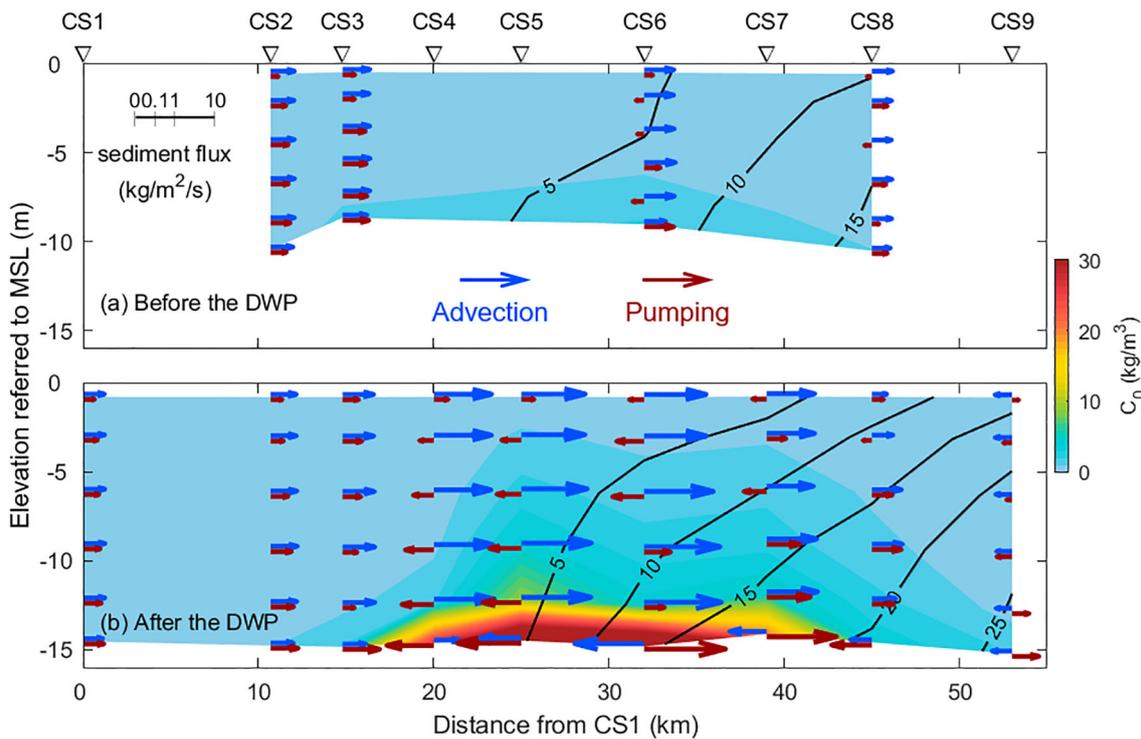**FIGURE 10**
Along-channel sediment fluxes driven by advection (blue) and pumping (red) before **(a)** and after **(b)** the Deep Waterway Project (DWP). Positive values indicate seaward transport, while negative values represent landward transport. Black lines denote isohalines, and the filled colors represent tidally averaged suspended sediment concentrations.
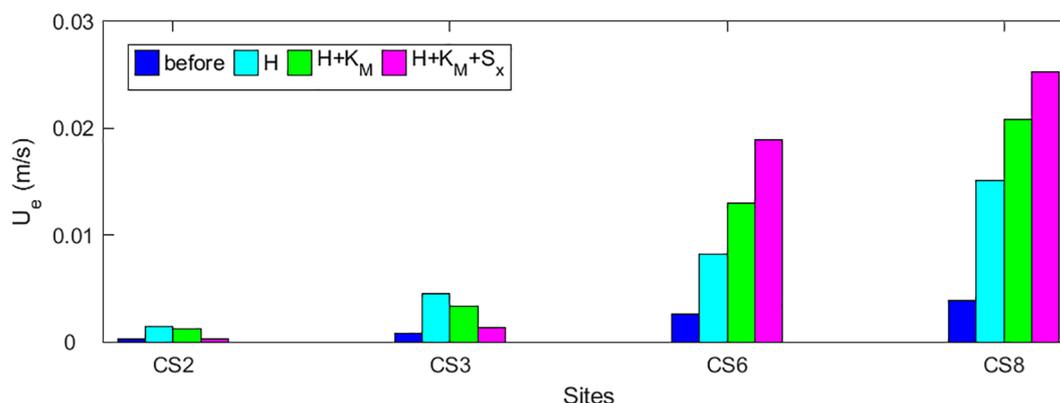
FIGURE 11
Analysis of the contributions of channel depth (H), eddy viscosity (K_M), and along-channel salinity gradient (S_x) to estuarine circulation (U_e) by Equation 12. Blue bars represent estimated U_e before the Deep Waterway Project (DWP), using pre-DWP values of H, K_M, and S_x. Cyan bars show the estimates with H after the DWP, while K_M and S_x remain unchanged, highlighting the effect of increased depth. Green bars represent estimates incorporating post-DWP K_M, allowing comparison with cyan bars to assess the impact of eddy viscosity. Finally, magenta bars represent post-DWP estimates using all updated parameters, with the difference between magenta and green bars indicating the contribution of changes in S_x.

which was previously weak, became more prominent, particularly around the ETM zone. At CS4, tidal pumping transported sediment upstream, while at CS6–CS7, it shifted sediment downstream. This bidirectional effect contributed to the elongation of the ETM.

At CS8, tidal pumping induced seaward sediment transport in the middle layers while driving landward transport near the bottom, reinforcing sediment accumulation. The interaction between advection and tidal pumping resulted in a net convergence of sediment in the mid-estuary, supporting the growth and persistence of ETM.

4.5.3 Formation and expansion of the ETM

The intensified estuarine circulation and increased sediment retention after the DWP facilitated the concentration and expansion of the ETM. Before the DWP, the ETM was relatively compact (~30 km in length) and maintained moderate SSCs (<5 kg/m³). After the DWP, the ETM extended to ~45 km, with near-bed SSCs increasing nearly 20-fold (Figure 3).

This transformation can be attributed to two key mechanisms:

1. Stratification-Enhanced Sediment Trapping: The strengthened density stratification after the DWP suppressed vertical mixing, allowing fine sediments to accumulate near the bed. This process reinforced sediment retention and limited seaward transport.
2. Tidal Pumping Redistribution: The increased velocity and SSC gradients enhanced dispersive fluxes, leading to sediment redistribution upstream and downstream of the ETM core. This process contributed to the ETM expansion while maintaining its position near the saltwater intrusion limit.

5 Discussion

5.1 Deepening and narrowing impacts on estuarine circulation

The observed increase in estuarine circulation post-DWP is primarily attributed to channel deepening and narrowing. Theoretical models suggest that estuarine circulation intensity (U_e) is governed by water depth (H), vertical mixing (represented by eddy viscosity, K_M), and the along-channel salinity gradient ($\frac{\partial S}{\partial x}$) (Hansen and Rattray, 1965; MacCready and Geyer, 2010; Ralston and Geyer, 2019). This section discusses their roles in the enhanced estuarine circulation due to the DWP.

Since estuarine circulation scales with H^3 (Equation 12; Hansen and Rattray, 1965; MacCready and Geyer, 2010), the deepening of the navigation channel, with a 50% increase in H, led to a threefold increase in U_e (Figure 11). Increased water depth with a fixed estuary width lowers flow velocity and friction velocity, thereby decreasing eddy viscosity and enhancing estuarine circulation intensity. This was the case for the lower reaches at CS6 and CS8, while the eddy viscosity increased, and estuarine circulation weakened in the upper reaches at CS2 and CS3 (Figure 11). Additionally, Channel deepening is expected to enhance salt intrusion and thereby return a lower along-channel salinity gradient (Hansen and Rattray, 1965; MacCready and Geyer, 2010; Ralston and Geyer, 2019). In the North Passage, however, $\frac{\partial S}{\partial x}$ decreased at CS2 and CS3, but increased in the lower reaches (e.g., CS6 and CS8; Figure 5e). Correspondingly, U_e declined in the upper reaches but increased in the lower reaches when including changes in $\frac{\partial S}{\partial x}$ (Figure 11). These deviations from expected deepening consequences highlight the impacts of narrowing on estuarine circulation.

Channel narrowing has three primary impacts on estuarine hydrodynamics: (1) increasing flow velocity by reducing cross-section area, (2) enhancing stratification by increasing freshwater flushing near the surface, and (3) raising along-channel salinity gradient by suppressing salt intrusion. In the upper reaches (CS2 and CS3) of the North Passage, where water columns were well-mixed and thereby stratification effect is negligible, increased eddy viscosity (K_M) is attributed to increasing flow (friction) velocity (Figures 4k, 5c), leading to a weakened estuarine circulation when including changes in K_M (Figure 11). Narrowing could enhance estuarine circulation by increasing stratification and the along-channel salinity gradient. In the downstream reaches, for example, the reduction in eddy viscosity is attributed to intensified stratification induced by both deepening and narrowing. Narrowing increases seaward freshwater flushing near the surface, whereas deepening facilitates saltwater intrusion in the bottom layer, thereby producing stronger stratification. Increased stratification (Ri) reduces eddy viscosity, and thus gives stronger circulation (Figure 11).

Narrowing of the North Passage, primarily due to the construction of dikes and deposition in groin fields, increases $\frac{\partial S}{\partial x}$ in two ways. First, the reduction in the cross-sectional area intensified freshwater flushing in the upper reaches, effectively shifting the saltwater seaward. Second, local hydraulic structures, such as dikes and groins, increased form drag and hydrodynamic resistance, constraining saltwater intrusion (Song and Wang, 2013; Zhu et al., 2021a). This restriction maintained the overall length of salt intrusion while increasing $\frac{\partial S}{\partial x}$. Consequently, estuarine circulation was enhanced in the lower reaches, where the strengthened salinity gradient promoted landward baroclinic pressure gradients and intensified exchange flows.

In addition to along-channel effects, estuarine narrowing also enhances stratification through lateral processes. One key mechanism involves groin fields, which trap saltwater during flood tides. During ebb tides, the faster-moving water in the main channel creates pronounced lateral salinity gradients between the deep channel and the adjacent shoals (Zhu et al., 2018b, 2020, 2021b; Zhou et al., 2019; Chen et al., 2020). This lateral salinity gradient drives a secondary circulation pattern, transporting saltier water from the groin fields toward the main channel near the bed. This process, known as lateral straining, strengthens density stratification within the estuary (Zhu et al., 2018b; Chen et al., 2020). Overall, the combined effects of deepening and narrowing played a crucial role in intensifying estuarine circulation, with narrowing influencing both mixing processes and salinity distribution.

5.2 Sediment import by estuarine circulation

The enhancement of estuarine circulation following the DWP was critical in increasing sediment import and retention within the North Passage. The strengthened two-layer flow structure, characterized by intensified seaward transport in the surface layer and landward transport near the bed, facilitated the accumulation of suspended sediment at the saltwater intrusion limit. This section discusses how estuarine circulation, modulated by increased stratification, contributed to enhanced sediment trapping.

The decomposition of sediment flux components (Figure 7) reveals that estuarine circulation became a dominant driver of sediment transport after the DWP. Before the DWP, barotropic forces primarily controlled sediment fluxes, with relatively weak contributions from circulation-driven transport. After the DWP, however, landward sediment transport associated with estuarine circulation intensified, particularly in the middle reaches of the estuary. The increase in near-bed inflows transported fine sediments upstream, leading to sediment convergence at the saltwater intrusion limit and contributing to the expansion of ETM.

The post-DWP increase in density stratification directly impacted sediment transport mechanisms. Enhanced salinity and sediment-induced stratification increased the gradient Richardson number (Ri) (Figure 4j), which in turn reduced vertical turbulent mixing (Toorman et al., 2002; Winterwerp, 2002; Xu, 2009; Ge et al., 2018). Stratification-induced suppression of vertical mixing facilitated the formation of high-concentration near-bed sediment layers. With SSCs exceeding 80 kg/m³ in certain regions, these concentrated benthic suspensions played a crucial role in sediment trapping. The development of concentrated benthic suspensions can be attributed to two interconnected processes. First, vertical mixing was further inhibited as density stratification increased, preventing sediment resuspension and favoring near-bed accumulation (Winterwerp, 2002; Dijkstra et al., 2018; Ge et al., 2018; Lin et al., 2021). This positive feedback loop reinforced sediment trapping, sustaining high SSCs near the bottom. Second, the strengthened estuarine circulation transported concentrated benthic suspensions landward, leading to significant sediment import and deposition in the mid-estuary. This transport pattern differed from tide-dominated estuaries, where tidal pumping is the primary mechanism for sediment import (Winterwerp, 2011; van Maren et al., 2015b; Dijkstra et al., 2019b; Dijkstra and de Goede, 2024).

The intensified estuarine circulation and the formation of concentrated benthic suspensions collectively contributed to sediment trapping at the saltwater intrusion limit. This process played a central role in reshaping sediment transport pathways and sustaining the ETM in the deepened and narrowed North Passage.

5.3 ETM extension by tidal pumping

The ETM in the North Passage expanded significantly following the DWP, showing increases in both spatial extent and SSC. Tidal pumping played a crucial role by redistributing fine sediments and enhancing sediment trapping. Combined with intensified stratification and stronger estuarine circulation, the enhanced tidal asymmetry post-DWP facilitated both a landward shift and a seaward extension of the ETM.

Tidal pumping mechanisms, in addition to periodic stratification, are influenced by velocity asymmetry, temporal and spatial lags, and dispersive fluxes, collectively contributing to

sediment redistribution (Simpson et al., 1990; Gatto et al., 2017; Wünsche et al., 2024). Following the DWP, tidal pumping intensified significantly, particularly in the middle reaches of the North Passage (Figure 9). This enhancement facilitated the redistribution of sediment trapped around the saltwater intrusion limit, promoting both upstream and downstream sediment transport. Spatial lag effects and dispersive flux emerged as critical mechanisms facilitating this sediment divergence.

Hydrodynamic changes induced by the DWP produced pronounced along-estuary velocity gradients. The greatest flow velocities and hydrodynamic energy were observed in the middle reaches (between stations CS4 and CS6), while velocities diminished upstream and downstream (Figure 4g). This uneven velocity distribution generated spatial lag effects, where sediment transport preferentially occurred from regions of higher energy to lower energy zones, resulting in sediment redistribution both seaward and landward (Friedrichs, 2011; Gatto et al., 2017). Consequently, this process actively contributed to ETM elongation and persistence.

In parallel, sediment trapping driven by estuarine circulation enhanced SSC in the mid-estuarine regions, producing significant along-channel SSC gradients (Figure 10b). These gradients reached values as high as 1.0 kg/m^4, elevating the significance of horizontal diffusion, often considered negligible in simpler tidal basins (Pritchard, 2005; Gatto et al., 2017). Horizontal diffusion, driven

by strong SSC gradients, induced net dispersive sediment fluxes from high-concentration zones towards lower-concentration areas, contributing further to the bidirectional ETM extension.

Quantifying the precise contribution of horizontal diffusion to sediment transport with field data alone remains challenging due to spatial and temporal resolution limitations. Common analytical methods for estimating horizontal diffusion include the gradient-flux approach, involving detailed field measurements of velocity and concentration gradients (Geyer and Nepf, 1996; Ralston and Stacey, 2007), or numerical modeling techniques capable of directly simulating advective and diffusive fluxes under controlled conditions (Burchard et al., 2018; Ralston and Geyer, 2019). Such numerical modeling approaches, integrating hydrodynamics with sediment transport modules, have been successfully applied in other estuaries (Ralston et al., 2012; Jalón-Rojas et al., 2021) and are highly recommended for future research on the Changjiang Estuary. These models could explicitly quantify the horizontal diffusion term, distinguishing its relative importance alongside advective and gravitational circulation-driven fluxes, thus offering a more comprehensive understanding of sediment dynamics within engineered estuaries.

Overall, spatial lag effects by velocity gradients and dispersive flux driven by SSC gradients were critical to the ETM expansion following the DWP. These processes effectively redistributed
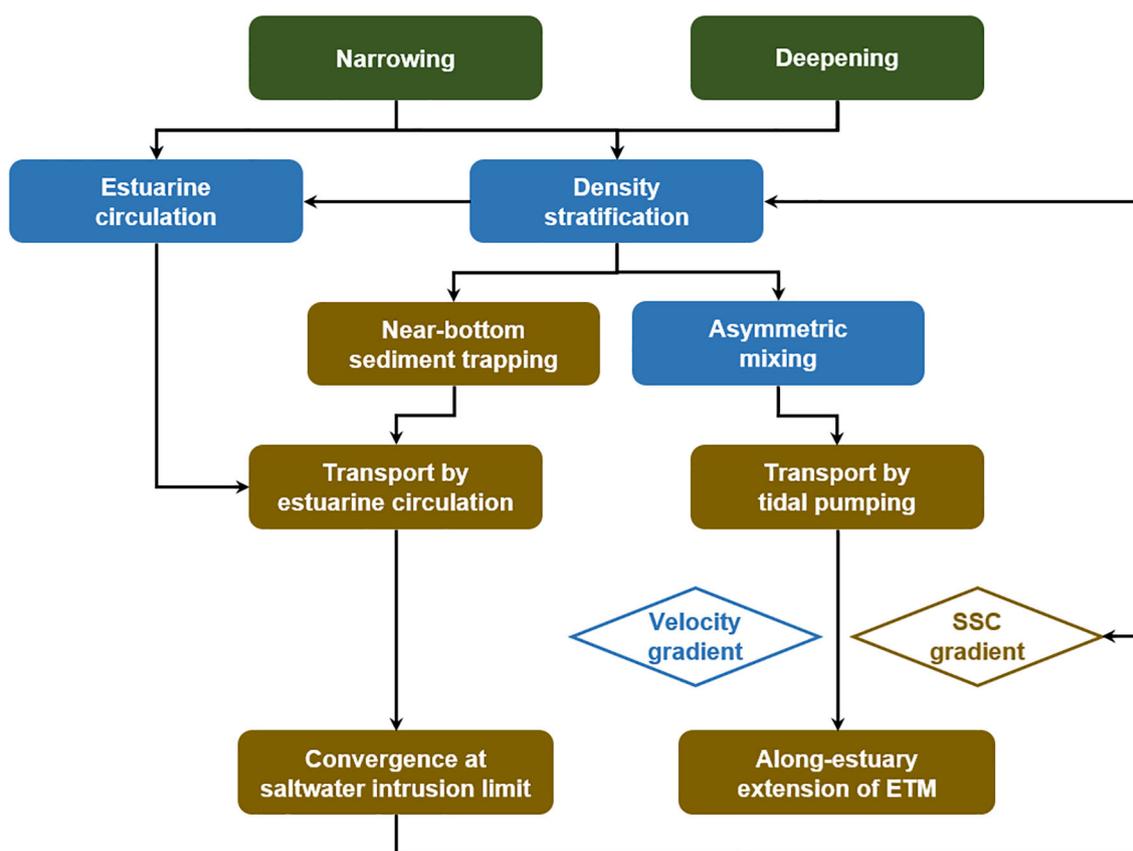

FIGURE 12
The cause-and-effect flow chart illustrates sediment transport and estuarine turbidity maximum (ETM) evolution in response to channel deepening and narrowing in the North Passage.

sediments both landward and seaward, underpinning the elongation and intensification of the ETM. A conceptual overview of these mechanisms and their interactions within the modified North Passage is summarized in Figure 12.

5.4 Impacts of declined fluvial sediment supply

In addition to the impacts of the DWP, the declined fluvial sediment supply can trigger substantial regime shifts in estuarine hydrodynamics, sediment dynamics and morphology (Luo et al., 2012, 2022; Wang et al., 2015; Guo et al., 2021b; Luan et al., 2021; Zhu et al., 2021a). A disruption in the sediment balance, resulting from reduced riverine input, potentially prompts increased sediment import from marine sources, influencing the ETM evolution. The sediment load at Datong has decreased by ~70% from the 1980s through the 2010s (Guo et al., 2019). Nonetheless, the Changjiang Estuary exhibits a delayed response to this dramatic sediment decline due to sediment replenishment from downstream channel erosion and the estuarine buffering capacity (Zhu et al., 2019; Guo et al., 2021a). Spatial variability in estuarine SSC responses further complicates this picture. For example, at Xuliujing, located near the upstream entrance of the estuary, surface SSC remained relatively stable until 2010, after which it began to decline (Chen et al., 2022). Conversely, in the ETM region, bathymetric changes showed an approximate 30-year lag relative to riverine sediment reductions, excluding the effects of dredging associated with the DWP (Zhu et al., 2019). Surface SSC in the ETM region declined since the early 2000s, corresponding with a roughly 20% reduction in the spatial extent of ETM (Jiang et al., 2013b; Luo et al., 2022). This reduction became particularly pronounced post-DWP, as increased stratification suppressed vertical mixing, limiting sediment transport into upper water layers (Figure 6).

However, despite the significant drop in fluvial sediment load, the near-bed SSC markedly increased in the North Passage, rising from a few kg/m^3 in the 1990s to tens of kg/m^3 in the 2010s (Wan

and Zhao, 2017; Ge et al., 2018; Lin et al., 2020, 2021). This unexpected increase in SSC under reduced riverine sediment supply highlights the critical role of marine-derived sediments, primarily sourced from local and delta-front erosion (Zhu et al., 2016, 2019). The correlation between decreased riverine sediment load and increased siltation since the DWP is evident from the temporal comparison of sediment load at Datong Station and annual siltation volumes within the North Passage (Figure 13). Marine sediment supply, therefore, emerges as a key contributor to the observed hyper-turbidity and ETM expansion in the North Passage post-DWP.

These observations imply that, while the DWP predominantly altered hydrodynamics and sediment transport from 1999 to 2012, the ongoing sediment reductions from upstream must be carefully considered in long-term predictions of hydrodynamic conditions and ETM evolution. Future numerical modeling studies should aim to explicitly differentiate and quantify the individual effects of declining fluvial sediment supply and anthropogenic interventions such as the DWP.

5.5 Limitations and implications

This study sheds light on how channel deepening and narrowing alter estuarine circulation, stratification, and sediment transport. However, our analysis has several limitations. First, parameters such as water depth (H), eddy viscosity (K_M), and along-channel salinity gradient ($\frac{\partial S}{\partial x}$) employed in our calculations represent cross-sectionally and tidally averaged values. The direct measurements analyzed in this study were collected primarily from the main navigation channel, assuming representativeness for the whole cross-section. Although this assumption is reasonable given the relatively uniform characteristics of the North Passage (~10 m depth and 7 km width, Figure 1), a more precise quantification would necessitate numerical models that capture full cross-sectional variability. Recent modeling studies have highlighted the profound effect of deepening on estuarine dynamics (e.g., along-estuary salinity gradient, stratification, estuarine circulation, and sediment
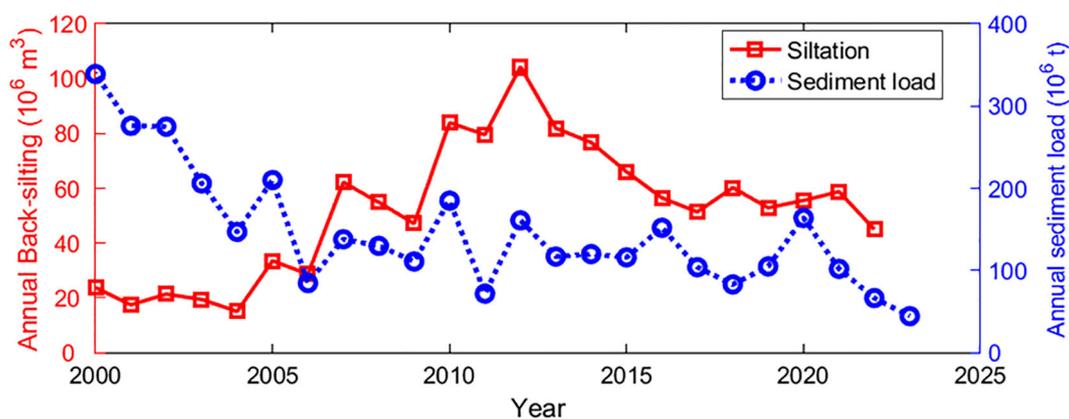

FIGURE 13
Annual sediment load at Datong Station and annual siltation in the North Passage (2000~2023).

transport), emphasizing the need for such detailed simulations (Jalón-Rojas et al., 2021; Grasso and Caillaud, 2023; Dijkstra and de Goede, 2024). Moreover, future modeling efforts should explore differential responses of sediment transport between the main channel and shallow shoals, improving our understanding of the impact of channel modifications.

Second, the friction velocity ($u_\star$), a key parameter in eddy viscosity estimation, was obtained by fitting the von Kármán-Prandtl velocity profile based on flow velocities measured at six relative depth layers. This approach likely overestimates friction velocities under significant sediment-induced stratification (Wright et al., 1999; Kim et al., 2000). The pronounced sediment-induced stratification at CS6 and CS8 suggests our eddy viscosity estimates may be inflated, consequently underestimating estuarine circulation. Future work should employ advanced turbulence methods, such as the turbulent kinetic energy method (Kim et al., 2000; Lin et al., 2021; Zhou et al., 2025), requiring high-frequency near-bed velocity measurements to enhance accuracy.

Additionally, a critical limitation arises from the absence of bottom sediment data during the survey periods. Observations from other studies indicate a shift towards finer sediment after the DWP, despite declining fluvial sediment supply. Specifically, bottom sediment grain sizes decreased from 69 μm in 1982 to 44~60 μm in 2003, and further to 10~25 μm in 2015 (Lou, 2005; Liu et al., 2010; Qiao et al., 2020); concurrently, suspended sediment grain sizes declined from 6.8 μm (pre-DWP) to 5.3 μm (post-DWP) (Chen et al., 2019; Yu et al., 2021). These grain size changes suggest shifts in sediment sources and increased marine sediment input. The feedback between bottom sediment properties and hydrodynamic variations, particularly under varying width-depth conditions, remains underexplored and represents an important research direction. Numerical modeling studies are particularly recommended to investigate these feedback mechanisms, further elucidating sediment transport processes.

This study demonstrates that enhanced estuarine circulation is the dominant driver of sediment import from the ocean following channel deepening and narrowing in a relatively river-dominated estuary. Intensified circulation significantly promotes sediment trapping at the saltwater intrusion limit, forming a positive feedback loop involving intensified flow velocity, increased stratification, turbulence damping, and hindered settling. This feedback loop results in extremely high near-bed SSCs, reducing benthic light penetration and contributing to hypoxia (low oxygen levels) conditions detrimental to estuarine ecology (Talke et al., 2009; Winterwerp et al., 2017; Schmidt et al., 2019). Furthermore, elevated SSCs increase channel siltation, necessitating frequent maintenance dredging with substantial economic implications (Liu et al., 2011a, 2019; de Nijs and Pietrzak, 2012). Thus, integrated management strategies balancing ecological and navigational requirements are critically important in engineered estuaries.

Finally, our findings underscore the critical influence of channel width on estuarine stratification, circulation, and sediment transport. Contrary to initial expectations of enhanced sediment flushing through narrowing (as commonly observed in river systems), narrowing by the DWP in the North Passage increased

sediment import via intensified estuarine circulation and stratification. Strengthened stratification promotes near-bed sediment trapping and the formation of concentrated benthic suspensions, which are transported landward by intensified near-bed inflows. Although narrowing enhanced sediment export driven by barotropic flows, the stronger estuarine circulation-induced sediment import ultimately led to net sediment convergence at the saltwater intrusion limit. As a result, post-DWP siltation rates (120 Mt) far exceeded initial predictions (30 Mt) (Wan, 2015; Liu et al., 2019). Similar width-controlled sediment transport dynamics, albeit predominantly via tidal pumping, have been observed in tide-dominated estuaries such as the Ems Estuary (van Maren et al., 2016) and the North Branch of the Changjiang Estuary (Guo et al., 2022). Thus, estuary width emerges as a universal critical parameter controlling sediment transport processes, albeit through differing mechanisms depending on the dominance of river discharge or tidal forces.

The sediment import mechanisms in engineered estuaries fundamentally depend on the relative influence of river discharge versus tidal forcing, which can be systematically characterized using the dimensionless Canter-Cremers number (N). In tide-dominated estuaries with small N values (e.g., Ems Estuary, $N \approx 0.005$), tidal pumping predominantly drives sediment import, supported by strong tidal asymmetries and sediment-induced drag reduction (Winterwerp, 2011; van Maren et al., 2015b; Dijkstra et al., 2019b). Conversely, in river-dominated estuaries such as the Changjiang Estuary ($N \approx 0.5$), sediment import primarily occurs through enhanced estuarine circulation triggered by deepening and narrowing. In these systems, gravitational circulation significantly outweighs tidal pumping in transporting sediment landward. These contrasting mechanisms underscore the complexity and diversity of estuarine responses to engineering interventions. Future global analyses are needed to comprehensively categorize estuaries across a spectrum of N values, systematically comparing sediment dynamics and regime shifts to support better-informed management strategies.

6 Conclusions

This study investigated the effects of channel deepening and narrowing on estuarine circulation, stratification, and sediment transport in the North Passage of the Changjiang Estuary. Our findings emphasize the crucial role of estuarine circulation and highlight the unexpected impacts of channel narrowing on sediment dynamics.

1. Deepening enhances estuarine circulation and sediment import. Increased water depth due to deepening strengthened the two-layer estuarine circulation by enhancing landward near-bed flow, promoting oceanic sediment import and intensified sediment trapping at the saltwater intrusion limit.

2. Narrowing modifies salinity gradients and strengthens stratification. While deepening alone typically extends salt

intrusion, concurrent narrowing imposed by hydraulic structures counteracted this effect. Enhanced hydraulic friction restricted salt intrusion and steepened the salinity gradients, particularly near the estuary mouth, which intensified stratification, suppressed vertical mixing, and reinforced estuarine circulation.

3. Stronger stratification enhances near-bed sediment trapping. Enhanced stratification suppressed turbulent mixing, facilitating concentrated benthic suspensions. The strengthened estuarine circulation subsequently transported these suspensions landward, maintaining elevated SSC at the saltwater intrusion limit.

4. Tidal pumping extends the ETM. Hydrodynamic changes following channel modifications intensified tidal pumping, especially in mid-estuary regions. Enhanced velocity gradients and spatial lag effects promoted sediment transport from high-energy to low-energy zones, extending the ETM.

These findings underscore the complex interplay between deepening, narrowing, and sediment dynamics. Contrary to expectations that narrowing might enhance sediment flushing, our results show it increased estuarine circulation and sediment trapping, leading to greater siltation. Similar processes observed in estuaries such as the Ems Estuary and the North Branch of the Changjiang Estuary further indicate that estuarine width is critical, with distinct mechanisms (estuarine circulation or tidal pumping) dominating in river- and tide-dominated systems, respectively.

The insights from this study have valuable implications for estuarine management and highlight the need for careful consideration of channel modifications. Future work employing high-resolution numerical modeling is recommended to quantify spatially detailed hydrodynamic and sediment processes and assess long-term morphological evolution resulting from ongoing estuarine interventions.

Data availability statement

The original contributions presented in the study are included in the article/supplementary material. Further inquiries can be directed to the corresponding author.

Author contributions

JL: Formal analysis, Writing – original draft, Visualization, Methodology, Funding acquisition, Conceptualization. Bv: Supervision, Writing – review & editing. CZ: Formal analysis, Writing – review & editing. LG: Formal analysis, Writing – review & editing. QH: Supervision, Project administration, Conceptualization, Writing – review & editing. ZW: Project administration, Writing – review & editing, Supervision. QY: Writing – review & editing.

Funding

Acknowledgments

Conflict of interest

The authors declare that the research was conducted in the absence of any commercial or financial relationships that could be construed as a potential conflict of interest.

Generative AI statement

The author(s) declare that no Generative AI was used in the creation of this manuscript.

Publisher's note

References

Blum, M. D., and Roberts, H. H. (2009). Drowning of the Mississippi Delta due to insufficient sediment supply and global sea-levelrise. *Nat. Geosci.* 2, 488–491. doi: 10.1038/ngeo553

Burchard, H., and Hofmeister, R. (2008). A dynamic equation for the potential energy anomaly for analysing mixing and stratification in estuaries and coastal seas. *Estuar. Coast. Shelf Sci.* 77, 679–687. doi: 10.1016/j.ecss.2007.10.025

Burchard, H., Schuttelaars, H. M., and Ralston, D. K. (2018). Sediment trapping in estuaries. *Ann. Rev. Mar. Sci.* 10, 371–395. doi: 10.1146/annurev-marine-010816-060535

Chen, Y., He, Q., Shen, J., and Du, J. (2020). The alteration of lateral circulation under the influence of human activities in a multiple channel system, Changjiang Estuary. *Estuar. Coast. Shelf Sci.* 242, 106823. doi: 10.1016/j.ecss.2020.106823

Chen, J., He, Q., Xie, W., and Guo, L. (2022). Characteristics of hydro-sediment changes in Xuliujing of Yangtze River Estuary after the Three Gorges Project operation. *J. Sediment Res.* 47, 60–66. doi: 10.16239/j.cnki.0468-155x.2022.03.009

Chen, Y., He, Q., Zhang, Y., and Lin, J. (2019). Grain size distribution of suspended sediment in Yangtze River estuary turbidity maximum in wet season. *J. Sediment Res.* 44, 48–55. doi: 10.16239/j.cnki.0468-155x.2019.05.008

Chu, N., Yao, P., Ou, S., Wang, H., Yang, H., and Yang, Q. (2022). Response of tidal dynamics to successive land reclamation in the Lingding Bay over the last century. *Coast. Eng.* 173, 104095. doi: 10.1016/j.coastaleng.2022.104095

Dai, Z., Liu, J. T., Wei, W., and Chen, J. (2014). Detection of the three gorges dam influence on the Changjiang (Yangtze River) submerged delta. *Sci. Rep.* 4, 6600. doi: 10.1038/srep06600

Day, J. W., Shaffer, G. P., Cahoon, D. R., and DeLaune, R. D. (2019). Canals, backfilling and wetland loss in the Mississippi Delta. *Estuar. Coast. Shelf Sci.* 227, 106325. doi: 10.1016/j.ecss.2019.106325

de Boer, G. J., Pietrzak, J. D., and Winterwerp, J. C. (2008). Using the potential energy anomaly equation to investigate tidal straining and advection of stratification in a region of freshwater influence. *Ocean Model.* 22, 1–11. doi: 10.1016/j.ocemod.2007.12.003

de Jonge, V. N., Schuttelaars, H. M., van Beusekom, J. E. E., Talke, S. A., and de Swart, H. E. (2014). The influence of channel deepening on estuarine turbidity levels and dynamics, as exemplified by the Ems estuary. *Estuar. Coast. Shelf Sci.* 139, 46–59. doi: 10.1016/j.ecss.2013.12.030

de Nijs, M. A. J., and Pietrzak, J. D. (2012). Saltwater intrusion and ETM dynamics in a tidally-energetic stratified estuary. *Ocean Model.* 49–50, 60–85. doi: 10.1016/j.ocemod.2012.03.004

Dijkstra, Y. M., and de Goede, R. J. A. (2024). Regime shift to hyperturbid conditions in the Loire Estuary: Overview of observations and model analysis of physical mechanisms. *J. Geophys. Res. Ocean.* 129, e2023JC020273. doi: 10.1029/2023JC020273

Dijkstra, Y. M., Schuttelaars, H. M., and Schramkowski, G. P. (2019a). A regime shift from low to high sediment concentrations in a tide-dominated estuary. *Geophys. Res. Lett.* 46, 4338–4345. doi: 10.1029/2019GL082302

Dijkstra, Y. M., Schuttelaars, H. M., Schramkowski, G. P., and Brouwer, R. L. (2019b). Modeling the transition to high sediment concentrations as a response to channel deepening in the Ems River Estuary. *J. Geophys. Res. Ocean.* 124, 1578–1594. doi: 10.1029/2018JC014367

Dijkstra, Y. M., Schuttelaars, H. M., and Winterwerp, J. C. (2018). The hyperturbid state of the water column in estuaries and rivers: The importance of hindered settling. *Ocean Dyn.* 68, 377–389. doi: 10.1007/s10236-018-1132-1

Dyer, K. R. (1974). The salt balance in stratified estuaries. *Estuar. Coast. Mar. Sci.* 2, 273–281. doi: 10.1016/0302-3524(74)90017-6

Friedrichs, C. T. (2011). "Tidal flat morphodynamics: A synthesis," in *Treatise on Estuarine and Coastal Science*. Eds. E. Wolanski and D. McLusky (Academic, Waltham, MA), 137–170.

Gatto, V. M., van Prooijen, B. C., and Wang, Z. B. (2017). Net sediment transport in tidal basins: Quantifying the tidal barotropic mechanisms in a unified framework. *Ocean Dyn.* 67, 1385–1406. doi: 10.1007/s10236-017-1099-3

Ge, J., Zhou, Z., Yang, W., Ding, P., Chen, C., Wang, Z. B., et al. (2018). Formation of concentrated benthic suspension in a time-dependent salt wedge estuary. *J. Geophys. Res. Ocean.* 123, 8581–8607. doi: 10.1029/2018JC013876

Geyer, W. R., and Nepf, H. (1996). "Tidal pumping of salt in a moderately stratified estuary," in *Buoyancy effects on coastal and estuarine dynamics*. Eds. D. G. Aubrey and C. T. Friedrichs (Washington: American Geophysical Union), 213–226. doi: 10.1029/ce053p0213

Grasso, F., and Caillaud, M. (2023). A ten-year numerical hindcast of hydrodynamics and sediment dynamics in the Loire Estuary. *Sci. Data* 10, 394. doi: 10.1038/s41597-023-02294-w

Grasso, F., and Le Hir, P. (2019). Influence of morphological changes on suspended sediment dynamics in a macrotidal estuary: Diachronic analysis in the Seine Estuary (France) from 1960 to 2010. *Ocean Dyn.* 69, 83–100. doi: 10.1007/s10236-018-1233-x

Guo, X., Fan, D., Zheng, S., Wang, H., Zhao, B., and Qin, C. (2021b). Revisited sediment budget with latest bathymetric data in the highly altered Yangtze (Changjiang) Estuary. *Geomorphology* 391, 107873. doi: 10.1016/j.geomorph.2021.107873

Guo, C., He, Q., Guo, L., and Winterwerp, J. C. (2017). A study of *in-situ* sediment flocculation in the turbidity maxima of the Yangtze Estuary. *Estuar. Coast. Shelf Sci.* 191, 1–9. doi: 10.1016/j.ecss.2017.04.001

Guo, L., Su, N., Townend, I., Wang, Z. B., Zhu, C., Wang, X., et al. (2019). From the headwater to the delta: A synthesis of the basin-scale sediment load regime in the Changjiang River. *Earth-Science Rev.* 197, 102900. doi: 10.1016/j.earscirev.2019.102900

Guo, L., Su, N., Zhu, C., and He, Q. (2018). How have the river discharges and sediment loads changed in the Changjiang River basin downstream of the Three Gorges Dam? *J. Hydrol.* 560, 259–274. doi: 10.1016/j.jhydrol.2018.03.035

Guo, L., van der Wegen, M., Jay, D. A., Matte, P., Wang, Z. B., Roelvink, D., et al. (2015). River-tide dynamics: Exploration of nonstationary and nonlinear tidal behavior in the Yangtze River estuary. *J. Geophys. Res. Ocean.* 120, 3499–3521. doi: 10.1002/2014JC010491

Guo, L., Xie, W., Xu, F., Wang, X., Zhu, C., Meng, Y., et al. (2022). A historical review of sediment export-import shift in the North Branch of Changjiang Estuary. *Earth Surf. Process. Landforms* 47, 5–16. doi: 10.1002/esp.5084

Guo, L., Zhu, C., Xie, W., Xu, F., Wu, H., Wan, Y., et al. (2021a). Changjiang Delta in the Anthropocene: Multi-scale hydro-morphodynamics and management challenges. *Earth-Science Rev.* 223, 103850. doi: 10.1016/j.earscirev.2021.103850

Hansen, D. V., and Rattray, M. (1965). Gravitational circulation in straits and estuaries. *J. Mar. Res.* 23, 104–122.

Jalón-Rojas, I., Dijkstra, Y. M., Schuttelaars, H. M., Brouwer, R. L., Schmidt, S., and Sottolichio, A. (2021). Multidecadal evolution of the turbidity maximum zone in a macrotidal river under climate and anthropogenic pressures. *J. Geophys. Res. Ocean.* 126, e2020JC016273. doi: 10.1029/2020JC016273

Jiang, C., de Swart, H. E., Li, J., and Liu, G. (2013a). Mechanisms of along-channel sediment transport in the North Passage of the Yangtze Estuary and their response to large-scale interventions. *Ocean Dyn.* 63, 283–305. doi: 10.1007/s10236-013-0594-4

Jiang, X., Lu, B., and He, Y. (2013b). Response of the turbidity maximum zone to fluctuations in sediment discharge from river to estuary in the Changjiang Estuary (China). *Estuar. Coast. Shelf Sci.* 131, 24–30. doi: 10.1016/j.ecss.2013.07.003

Kim, S.-C., Friedrichs, C. T., Maa, J. P. Y., and Wright, L. D. (2000). Estimating bottom stress in tidal boundary layer from acoustic Doppler velocimeter data. *J. Hydraul. Eng.* 126, 399–406. doi: 10.1061/(ASCE)0733-9429(2000)126:6(399

Li, L., He, Z., Xia, Y., and Dou, X. (2018). Dynamics of sediment transport and stratification in Changjiang River Estuary, China. *Estuar. Coast. Shelf Sci.* 213, 1–17. doi: 10.1016/j.ecss.2018.08.002

Li, X., Zhu, J., Yuan, R., Qiu, C., and Wu, H. (2016). Sediment trapping in the Changjiang Estuary: Observations in the North Passage over a spring-neap tidal cycle. *Estuar. Coast. Shelf Sci.* 177, 8–19. doi: 10.1016/j.ecss.2016.05.004

Lin, J., He, Q., Guo, L., van Prooijen, B. C., and Wang, Z. B. (2020). An integrated optic and acoustic (IOA) approach for measuring suspended sediment concentration in highly turbid environments. *Mar. Geol.* 421, 106062. doi: 10.1016/j.margeo.2019.106062

Lin, J., van Prooijen, B. C., Guo, L., Zhu, C., He, Q., and Wang, Z. B. (2021). Regime shifts in the Changjiang (Yangtze River) Estuary: The role of concentrated benthic suspensions. *Mar. Geol.* 433, 106403. doi: 10.1016/j.margeo.2020.106403

Liu, J., Cheng, H., Han, L., and Wang, Z. (2019). Interannual variations on siltation of the 12.5-m deepwater navigation channel in Yangtze Estuary. *Adv. Water Sci.* 30, 65–75. doi: 10.14042/j.cnki.32.1309.2019.01.007

Liu, H., He, Q., Wang, Z., Weltje, G. J., and Zhang, J. (2010). Dynamics and spatial variability of near-bottom sediment exchange in the Yangtze Estuary, China. *Estuar. Coast. Shelf Sci.* 86, 322–330. doi: 10.1016/j.ecss.2009.04.020

Liu, G.f., Wu, H.l., Guo, W.h., Zhu, J.r., and Sun, L.c. (2011a). Dispersal and fate of dredged materials disposed of in the Changjiang Estuary determined by use of an in situ rare earth element tracer. *China Ocean Eng.* 25, 495–506. doi: 10.1007/s13344-011-0040-7

Liu, G., Zhu, J., Wang, Y., Wu, H., and Wu, J. (2011b). Tripod measured residual currents and sediment flux: Impacts on the silting of the Deepwater Navigation Channel in the Changjiang Estuary. *Estuar. Coast. Shelf Sci.* 93, 192–201. doi: 10.1016/j.ecss.2010.08.008

Lou, F. (2005). *The sedimentary and accretion-erosion environment of the outer navigation channel in Changjiang Estuary* (East China Normal University). doi: 10.1016/j.regsciurbeco.2008.06.005%0Ahttps://www.researchgate.net/publication/305320484_SISTEM_PEMBETUNGAN_TERPUSAT_STRATEGI_MELESTARI

Luan, H. L., Ding, P. X., Wang, Z. B., Ge, J. Z., and Yang, S. L. (2016). Decadal morphological evolution of the Yangtze Estuary in response to river input changes and estuarine engineering projects. *Geomorphology* 265, 12–23. doi: 10.1016/j.geomorph.2016.04.022

Luan, H. L., Ding, P. X., Yang, S. L., and Wang, Z. B. (2021). Accretion-erosion conversion in the subaqueous Yangtze Delta in response to fluvial sediment decline. *Geomorphology* 382, 107680. doi: 10.1016/j.geomorph.2021.107680

Luo, W., Shen, F., He, Q., Cao, F., Zhao, H., and Li, M. (2022). Changes in suspended sediments in the Yangtze River Estuary from 1984 to 2020: Responses to basin and estuarine engineering constructions. *Sci. Total Environ.* 805, 150381. doi: 10.1016/j.scitotenv.2021.150381

Luo, X. X., Yang, S. L., and Zhang, J. (2012). The impact of the Three Gorges Dam on the downstream distribution and texture of sediments along the middle and lower Yangtze River (Changjiang) and its estuary, and subsequent sediment dispersal in the East China Sea. *Geomorphology* 179, 126–140. doi: 10.1016/j.geomorph.2012.05.034

MacCready, P., and Geyer, W. R. (2010). Advances in estuarine physics. *Ann. Rev. Mar. Sci.* 2, 35–58. doi: 10.1146/annurev-marine-120308-081015

Ministry of Water Resources the People's Republic of China (2024). *China River Sediment Bulletin 2023* (Beijing, China: China Water & Power Press). Available at: http://www.mwr.gov.cn/sj/tjgb/zghlnsgb.

Munk, W. H., and Anderson, E. R. (1948). Note on a theory of the thermocline. *J. Mar. Res.* 7, 276–295.

Peng, T., Tian, H., Singh, V. P., Chen, M., Liu, J., Ma, H., et al. (2020). Quantitative assessment of drivers of sediment load reduction in the Yangtze River basin, China. *J. Hydrol.* 580, 124242. doi: 10.1016/j.jhydrol.2019.124242

Pritchard, D. (2005). Suspended sediment transport along an idealised tidal embayment: Settling lag, residual transport and the interpretation of tidal signals. *Ocean Dyn.* 55, 124–136. doi: 10.1007/s10236-005-0004-7

Qiao, Y., He, Q., Wang, X., and Meng, Y. (2020). Study on surface sediment water-contents and its influence factors in the Yangtze Estuary. *J. Sediment Res.* 45, 29–36. doi: 10.16239/j.cnki.0468-155x.2020.01.005

Ralston, D. K., and Geyer, W. R. (2019). Response to channel deepening of the salinity intrusion, estuarine circulation, and stratification in an urbanized estuary. *J. Geophys. Res. Ocean.* 124, 4784–4802. doi: 10.1029/2019JC015006

Ralston, D. K., Geyer, W. R., and Warner, J. C. (2012). Bathymetric controls on sediment transport in the Hudson River estuary: Lateral asymmetry and frontal trapping. *J. Geophys. Res. Ocean.* 117, 1–21. doi: 10.1029/2012JC008124

Ralston, D. K., and Stacey, M. T. (2007). Tidal and meteorological forcing of sediment transport in tributary mudflat channels. *Cont. Shelf Res.* 27, 1510–1527. doi: 10.1016/j.csr.2007.01.010

Schmidt, S., Diallo, I. I., Derriennic, H., Fallou, H., and Lepage, M. (2019). Exploring the susceptibility of turbid estuaries to hypoxia as a prerequisite to designing a pertinent monitoring strategy of dissolved oxygen. *Front. Mar. Sci.* 6. doi: 10.3389/fmars.2019.00352

Shi, Z. (2004). Behaviour of fine suspended sediment at the North passage of the Changjiang Estuary, China. *J. Hydrol.* 293, 180–190. doi: 10.1016/j.jhydrol.2004.01.014

Simpson, J. H., Brown, J., Matthews, J., and Allen, G. (1990). Tidal straining, density currents, and stirring in the control of estuarine stratification. *Estuaries* 13, 125–132. doi: 10.2307/1351581

Song, D., and Wang, X. H. (2013). Suspended sediment transport in the Deepwater Navigation Channel, Yangtze River Estuary, China, in the dry season 2009. *J. Geophys. Res. Ocean* 2. doi: 10.1002/jgrc.20411

Su, J., and Wang, K. (1986). The suspended sediment balance in Changjiang estuary. *Estuar. Coast. Shelf Sci.* 23, 81–98. doi: 10.1016/0272-7714(86)90086-7

Talke, S. A., de Swart, H. E., and de Jonge, V. N. (2009). An idealized model and systematic process study of oxygen depletion in highly turbid estuaries. *Estuaries Coasts* 32, 602–620. doi: 10.1007/s12237-009-9171-y

Talke, S. A., and Jay, D. A. (2020). Changing tides: The role of natural and anthropogenic factors. *Ann. Rev. Mar. Sci.* 12, 121–151. doi: 10.1146/annurev-marine-010419-010727

Toorman, E. A., Bruens, A. W., Kranenburg, C., and Winterwerp, J. C. (2002). Interaction of suspended cohesive sediment and turbulence. *Proc. Mar. Sci.* 5, 7–23. doi: 10.1016/S1568-2692(02)80005-5

van Maren, D. S., Beemster, J. G. W., Wang, Z. B., Khan, Z. H., Schrijvershof, R. A., and Hoitink, A. J. F. (2023). Tidal amplification and river capture in response to land reclamation in the Ganges-Brahmaputra delta. *Catena* 220, 106651. doi: 10.1016/j.catena.2022.106651

van Maren, D. S., Oost, A. P., Wang, Z. B., and Vos, P. C. (2016). The effect of land reclamations and sediment extraction on the suspended sediment concentration in the Ems Estuary. *Mar. Geol.* 376, 147–157. doi: 10.1016/j.margeo.2016.03.007

van Maren, D. S., van Kessel, T., Cronin, K., and Sittoni, L. (2015a). The impact of channel deepening and dredging on estuarine sediment concentration. *Cont. Shelf Res.* 95, 1–14. doi: 10.1016/j.csr.2014.12.010

van Maren, D. S., Winterwerp, J. C., and Vroom, J. (2015b). Fine sediment transport into the hyper-turbid lower Ems River: The role of channel deepening and sediment-induced drag reduction. *Ocean Dyn.* 65, 589–605. doi: 10.1007/s10236-015-0821-2

Wan, Y. (2015). *Multiscale physical processes of fine sediment in an estuary, Ph.D. thesis* (Delft University of Technology).

Wan, Y., and Zhao, D. (2017). Observation of saltwater intrusion and ETM dynamics in a stably stratified estuary: The Yangtze Estuary, China. *Environ. Monit. Assess.* 189, 89. doi: 10.1007/s10661-017-5797-6

Wang, Y., Shen, J., and He, Q. (2010). A numerical model study of the transport timescale and change of estuarine circulation due to waterway constructions in the Changjiang Estuary, China. *J. Mar. Syst.* 82, 154–170. doi: 10.1016/j.jmarsys.2010.04.012

Wang, Z. B., van Maren, D. S., Ding, P. X., Yang, S. L., van Prooijen, B. C., de Vet, P. L. M., et al. (2015). Human impacts on morphodynamic thresholds in estuarine systems. *Cont. Shelf Res.* 111, 174–183. doi: 10.1016/j.csr.2015.08.009

Wang, Z. B., Winterwerp, J. C., and He, Q. (2014). Interaction between suspended sediment and tidal amplification in the Guadalquivir Estuary. *Ocean Dyn.* 64, 1487–1498. doi: 10.1007/s10236-014-0758-x

Winterwerp, J. C. (2002). Scaling parameters for high-concentrated mud suspensions in tidal flow. *Proc. Mar. Sci.* 5, 171–186. doi: 10.1016/S1568-2692(02)80015-8

Winterwerp, J. C. (2011). Fine sediment transport by tidal asymmetry in the high-concentrated Ems River: Indications for a regime shift in response to channel deepening. *Ocean Dyn.* 61, 203–215. doi: 10.1007/s10236-010-0332-0

Winterwerp, J. C., Vroom, J., Wang, Z. B., Krebs, M., Hendriks, E. C. M., van Maren, D. S., et al. (2017). SPM response to tide and river flow in the hyper-turbid Ems River. *Ocean Dyn.* 67, 559–583. doi: 10.1007/s10236-017-1043-6

Winterwerp, J. C., and Wang, Z. B. (2013). Man-induced regime shifts in small estuaries-I: Theory. *Ocean Dyn.* 63, 1279–1292. doi: 10.1007/s10236-013-0662-9

Winterwerp, J. C., Wang, Z. B., van Braeckel, A., van Holland, G., and Kösters, F. (2013). Man-induced regime shifts in small estuaries-II: A comparison of rivers. *Ocean Dyn.* 63, 1293–1306. doi: 10.1007/s10236-013-0663-8

Wright, L. D., Kim, S.-C., and Friedrichs, C. T. (1999). Across-shelf variations in bed roughness, bed stress and sediment suspension on the northern California shelf. *Mar. Geol.* 154, 99–115. doi: 10.1016/S0025-3227(98)00106-6

Wu, Z., Zhao, D., Syvitski, J. P. M., Saito, Y., Zhou, J., and Wang, M. (2020). Anthropogenic impacts on the decreasing sediment loads of nine major rivers in China 1954–2015. *Sci. Total Environ.* 739, 139653. doi: 10.1016/j.scitotenv.2020.139653

Wünsche, A., Becker, M., Fritzsch, R., Kelln, J., and Winter, C. (2024). The sensitivity of tidal asymmetry descriptors in the Ems estuary. *Ocean Dyn.* 74, 613–627. doi: 10.1007/s10236-024-01622-x

Xu, J. (2009). *Study on near bottom dynamics and sediment processes in turbidity maximum, MSc thesis* (China: East China Normal University).

Yang, S. L., Milliman, J. D., Li, P., and Xu, K. (2011). 50,000 dams later: Erosion of the Yangtze River and its delta. *Glob. Planet. Change* 75, 14–20. doi: 10.1016/j.gloplacha.2010.09.006

Yu, S., He, Q., Chen, Y., and Deng, Z. (2021). Response of suspended sediment particle size to sediment reduction in the Yangtze Estuary turbidity maximum zone. *J. Sediment Res.* 46, 60–67. doi: 10. 16239/j.cnki.0468-155x.2021. 04. 010

Zhang, R., Chen, Y., Chen, P., Zhou, X., Chen, K., Sun, Z., et al. (2023). Impacts of tidal flat reclamation on suspended sediment dynamics in the tidal-dominated Wenzhou Coast, China. *Front. Mar. Sci.* 10. doi: 10.3389/fmars.2023.1097177

Zhang, M., Townend, I. H., Cai, H., and Zhou, Y. (2016). Seasonal variation of tidal prism and energy in the Changjiang River estuary: A numerical study. *Chin. J. Oceanol. Limnol.* 34, 219–230. doi: 10.1007/s00343-015-4302-8

Zhang, D., Xie, W., Shen, J., Guo, L., Chen, Y., and He, Q. (2022a). Sediment dynamics in the mudbank of the Yangtze River Estuary under regime shift of source and sink. *Int. J. Sediment Res.* 37, 97–109. doi: 10.1016/j.ijsrc.2021.07.005

Zhang, W., Xu, Y. J., Guo, L., Lam, N. S. N., Xu, K., Yang, S., et al. (2022b). Comparing the Yangtze and Mississippi River Deltas in the light of coupled natural-human dynamics: Lessons learned and implications for management. *Geomorphology* 399, 108075. doi: 10.1016/j.geomorph.2021.108075

Zhou, Z., Ge, J., Van Maren, D. S., Luan, H., Guo, W., Ma, J., et al. (2025). Multi-year observations of near-bed hydrodynamics and suspended sediment at the core of the estuarine turbidity maximum of the Changjiang Estuary. *Earth Syst. Sci. Data* 17, 917–935. doi: 10.5194/essd-17-917-2025

Zhou, Z., Ge, J., Wang, Z. B., van Maren, D. S., Ma, J., and Ding, P. (2019). Study of lateral flow in a stratified tidal channel-shoal system: The importance of intratidal salinity variation. *J. Geophys. Res. Ocean.* 124, 6702–6719. doi: 10.1029/2019JC015307

Zhu, L., Chen, X., and Wu, Z. (2021b). Alteration of estuarine circulation pattern due to channel modification in the North Passage of the Changjiang River Estuary. *Acta Oceanol. Sin.* 40, 162–172. doi: 10.1007/s13131-020-1674-1

Zhu, C., Guo, L., van Maren, D. S., Tian, B., Wang, X., He, Q., et al. (2019). Decadal morphological evolution of the mouth zone of the Yangtze Estuary in response to human interventions. *Earth Surf. Process. Landforms* 44, 2319–2332. doi: 10.1002/esp.4647

Zhu, C., Guo, L., van Maren, D. S., Wang, Z. B., and He, Q. (2021a). Exploration of decadal tidal evolution in response to morphological and sedimentary changes in the Yangtze Estuary. *J. Geophys. Res. Ocean.* 126, e2020JC017019. doi: 10.1029/2020JC017019

Zhu, L., He, Q., and Shen, J. (2018b). Modeling lateral circulation and its influence on the along-channel flow in a branched estuary. *Ocean Dyn.* 68, 177–191. doi: 10.1007/s10236-017-1114-8

Zhu, L., He, Q., and Shen, J. (2020). Response of stratification processes to tidal current alteration due to channel narrowing and deepening. *J. Geophys. Res. Ocean.* 125, 1–20. doi: 10.1029/2019JC015223

Zhu, L., He, Q., Shen, J., and Wang, Y. (2016). The influence of human activities on morphodynamics and alteration of sediment source and sink in the Changjiang Estuary. *Geomorphology* 273, 52–62. doi: 10.1016/j.geomorph.2016.07.025

Zhu, C., van Maren, D. S., Guo, L., Lin, J., He, Q., and Wang, Z. B. (2022). Feedback effects of sediment suspensions on transport mechanisms in an estuarine turbidity maximum. *J. Geophys. Res. Ocean.* 127, e2021JC018029. doi: 10.1029/2021JC018029

Zhu, C., van Maren, D. S., Guo, L., Xie, W., Xing, C., Wang, Z. B., et al. (2025). Water and sediment exchange between the anthropogenically modified distributaries of the Yangtze Estuary. *Catena* 250, 108729. doi: 10.1016/j.catena.2025.108729

Zhu, J., Wu, H., Li, L., and Qiu, C. (2018a). "Saltwater intrusion in the Changjiang estuary," in *Coastal Environment, Disaster, and Infrastructure - A Case Study of China's Coastline*. Eds. X. S. Liang and Y. Zhang (BoD-Books on Demand), 49–73. doi: 10.5772/intechopen.80903